Properties of orbital-selective Mott insulators within low-dimensional multiorbital systems

Dr. Jacek HERBRYCH

Faculty of Fundamental Problems of Technology
Wrocław University of Science and Technology

January 20, 2022

Contents

1 Basic info **1**
- 1.1 Personal data . . . 1
- 1.2 Education . . . 1
- 1.3 Employment history and scientific secondments . . . 2

2 Scientific achievement **3**
- 2.1 Title of scientific achievement . . . 3
- 2.2 Publications included in the scientific achievement . . . 3
  - Brief description and author contribution . . . 3
- 2.3 Description . . . 6
  - Introduction . . . 6
  - Static spin properties . . . 9
  - Dynamical spin properties . . . 16
  - Electronic properties . . . 20
  - Conclusions . . . 24
  - Bibliography . . . 25

3 Other scientific and research achievements **30**
- 3.1 JCR publication list . . . 30
  - Brief description . . . 33
- 3.2 Bibliometric information . . . 33
- 3.3 Research projects . . . 34
- 3.4 Participation in European programs . . . 34
- 3.5 Scientific talks . . . 35
  - Oral presentations . . . 35
  - Poster presentation . . . 36
  - Invited talks at the scientific institutions . . . 36
- 3.6 Membership in scientific societies . . . 36
- 3.7 Refereeing in international journals . . . 37
- 3.8 Scientific collaborations . . . 37

4 Didactic achievements and administrative activity **38**
- 4.1 Didactic activity . . . 38
- 4.2 Scientific supervision of students and PhD students . . . 38
- 4.3 Administrative activity . . . 38

Basic info

1.1 Personal data

Name and surname Jacek Herbrych

Work address Faculty of Fundamental Problems of Technology
Wrocław University of Science and Technology
Wyb. Wyspiańskiego 27
50-370 Wrocław, Poland

Phone +48 519 625 993

Email jacek.herbrych@pwr.edu.pl

Webpage https://herbrychjacek.bitbucket.io

ORCID 0000-0001-9860-2146

1.2 Education

PhD in Physics 2013
Faculty of Mathematics and Physics
University of Ljubljana, Slovenia

Title **Finite-temperature dynamics of quantum spin chains**

Adviser Prof. Dr. Peter Prelovšek

Committee Prof. Dr. Tomaž Prosen (University of Ljubljana)
Prof. Dr. Denis Arčon (Jožef Stefan Institute)
Prof. Dr. Xenophon Zotos (University of Crete)

MSc in Physics 2010
Faculty of Physics and Applied Informatics
University of Łódź, Poland

Title **Lorentz transformation in deformed Minkowski space**

Adviser Prof. Dr. Cezary Gonera

Committee Prof. Dr. Piotr Kosiński (University of Łódź)

1.3 Employment history and scientific secondments

since IV/2019 Assistant Professor
Faculty of Fundamental Problems of Technology
Wrocław University of Science and Technology
Wrocław, Poland

X/2016 - III/2019 Researcher
Materials Science and Technology Division
Oak Ridge National Laboratory
Oak Ridge, USA

X/2016 - III/2019 Researcher/Postdoc with Prof. Dr. Elbio Dagotto
Department of Physics and Astronomy
University of Tennessee
Knoxville, USA

I/2014 - VIII/2016 Researcher
Crete Center for Quantum Complexity and Nanotechnology
Heraklion, Greece

I/2014 - VI/2016 Researcher/Postdoc with Prof. Dr. Xenophon Zotos
Department of Physics
University of Crete
Heraklion, Greece

V/2012 Scientific secondment in Prof. Dr. Xenophon Zotos group
Foundation for Research and Technology - Hellas
Heraklion, Greece

X/2010 - XII/2013 Young Researcher
Department of Theoretical Physics
Jožef Stefan Institute
Ljubljana, Slovenia

Scientific achievement

2.1 Title of scientific achievement

Properties of orbital-selective Mott insulators within low-dimensional multiorbital systems

2.2 Publications included in the scientific achievement

H1 *Spin dynamics of the block orbital-selective Mott phase*,
J. Herbrych, N. Kaushal, A. Nocera, G. Alvarez, A. Moreo, and E. Dagotto,
Nat. Commun. **9**, 3736 (2018).

H2 *Novel Magnetic Block States in Low-Dimensional Iron-Based Superconductors*,
J. Herbrych, J. Heverhagen, N. D. Patel, G. Alvarez, M. Daghofer, A. Moreo, and E. Dagotto,
Phys. Rev. Lett. **123**, 027203 (2019).

H3 *Block-spiral magnetism: An exotic type of frustrated order*,
J. Herbrych, J. Heverhagen, G. Alvarez, M. Daghofer, A. Moreo, and E. Dagotto,
Proc. Natl. Acad. Sci. USA **117**, 16226 (2020).

H4 *Block orbital-selective Mott insulators: a spin excitation analysis*,
J. Herbrych, G. Alvarez, A. Moreo, and E. Dagotto,
Phys. Rev. B **102**, 115134 (2020).

H5 *Interaction-induced topological phase transition and Majorana edge states in low-dimensional orbital-selective Mott insulators*,
J. Herbrych, M. Środa, G. Alvarez, M. Mierzejewski, and E. Dagotto,
Nat. Commun. **12**, 2955 (2021).

H6 *Quantum magnetism of iron-based ladders: blocks, spirals, and spin flux*,
M. Środa, E. Dagotto, and J. Herbrych,
Phys. Rev. B **104**, 045128 (2021).

Brief description and author contribution

[H1] *Spin dynamics of the block orbital-selective Mott phase*,
J. Herbrych, N. Kaushal, A. Nocera, G. Alvarez, A. Moreo, and E. Dagotto,
Nat. Commun. 9, 3736 (2018)
This work presents a theoretical prediction for the dynamical spin structure factor $S(q,\omega)$ within a block orbital-selective Mott phase (OSMP), i.e., in the system of ferromagnetic spin "islands" which are antiferromagnetically coupled along the legs, $\uparrow\uparrow\downarrow\downarrow$. In agreement with inelastic neutron scattering (INS) experiments on the iron-based compounds,

two dominant features are found: low-energy dispersive and high-energy dispersionless modes. The former represents the spin-wave-like dynamics of the block ferromagnetic islands, while the latter is attributed to a novel type of local on-site spin excitations controlled by the Hund coupling.

Author contribution: I initiated the research project. I co-developed the density matrix renormalization group code and performed all the numerical simulations. I provided the interpretation of the research results, e.g., I identified the $q > \pi/2$ mode as a high-energy momentum-independent excitation. I designed the toy model for the acoustic and optical excitations. I have provided the Hund exchange analysis of the optical mode. Finally, I wrote most of the manuscript text. I estimate my contribution to this article to be $\sim$ 70%.

[H2] *Novel Magnetic Block States in Low-Dimensional Iron-Based Superconductors*,
J. Herbrych, J. Heverhagen, N. D. Patel, G. Alvarez, M. Daghofer, A. Moreo, and E. Dagotto,
Phys. Rev. Lett. 123, 027203 (2019)
The analysis presented in this work shows that the electron doping of the OSMP induces a whole class of novel block states beyond the previously reported $\uparrow\uparrow\downarrow\downarrow$ pattern with ordering wavevector $\pi/2$. Furthermore, the effective model of the multiorbital system within OSMP is presented, the so-called generalized Kondo-Heisenberg model.

Author contribution: I initiated the research project. I adapted the code and performed all of the numerical simulations. I provided the interpretation of the research results, e.g., I performed the analysis of the static spin structure factor. I developed and tested the hypothesis for the "stabilization of the Fermi instability", i.e., that the magnetic ordering follows the electronic density. I derived and tested the effective Hamiltonian, i.e., the generalized Kondo-Heisenberg model. I wrote most of the manuscript text. I estimate my contribution to this article to be $\sim$ 70%.

[H3] *Block-spiral magnetism: An exotic type of frustrated order*,
J. Herbrych, J. Heverhagen, G. Alvarez, M. Daghofer, A. Moreo, and E. Dagotto,
Proc. Natl. Acad. Sci. USA 117, 16226 (2020)
It is shown that the competing energy scales of the seemingly nonfrustrated OSMP within the low-dimensional multiorbital Hubbard model can originate a "block–chiral magnetism", i.e., a state with rigidly rotating spin–magnetic islands. By examining the behavior of the electronic degrees of freedom, parity-breaking quasiparticles are revealed.

Author contribution: I initiated the research project. I adapted the code and performed all of the numerical simulations. I provided the interpretation of the research results, e.g., I performed a detailed analysis of spin-spin correlation function and chirality correlation function. I build and tested the hypothesis for the block-spiral magnetic ordering via the dimer correlation function. I identified the parity breaking quasiparticles. I presented the phenomenological arguments for the effective spin Hamiltonian. I wrote most of the manuscript text. I estimate my contribution to this article to be $\sim$ 70%.

[H4] *Block orbital-selective Mott insulators: a spin excitation analysis*,
J. Herbrych, G. Alvarez, A. Moreo, and E. Dagotto,
Phys. Rev. B 102, 115134 (2020)
A comprehensive study of the spin excitations - measured by the dynamical spin structure factor $S(q, \omega)$ - of the block-magnetic state within low-dimensional orbital-selective Mott insulators is presented.

Author contribution: I initiated the research project. I adapted the code and performed all of

the numerical simulations. I provided the interpretation of the research results, e.g., I performed a detailed analysis of the spin spectra. I identified unique features of the block and block-spiral ordering, relevant for neutron scattering experimentalists. I co-developed the phenomenological effective spin model for the block magnetism. I wrote most of the manuscript text. I estimate my contribution to this article to be $\sim 70\%$.

[H5] ***Interaction-induced topological phase transition and Majorana edge states in low-dimensional orbital-selective Mott insulators*,**
J. Herbrych, M. Środa, G. Alvarez, M. Mierzejewski, and E. Dagotto,
Nat. Commun. 12, 2955 (2021)
This work shows that the Coulomb electron-electron interaction can drive a topologically trivial canonical superconductor with orbital degrees of freedom into the topologically nontrivial state. Namely, it's shown that above a critical value of the Hubbard interaction, the system simultaneously develops spiral spin order, a highly unusual triplet amplitude in superconductivity, and zero-energy Majorana modes at the edges of the system.

Author contribution: I initiated the research project. I adapted the code and performed all of the numerical simulations. I provided the interpretation of the research results, e.g., performed the analysis of the single-particle spectral function and local density-of-states. I build and tested the hypothesis that topological phase transition is driven by the magnetic properties of the system. I developed the arguments for the presence of the zero-energy Majorana modes (e.g., the behavior of the entanglement entropy, the emergence of the triplet superconducting order parameter, the emergence of weight in the local density-of-states). I wrote most of the manuscript text. I estimate my contribution to this article to be $\sim 70\%$.

[H6] ***Quantum magnetism of iron-based ladders: blocks, spirals, and spin flux*,**
M. Środa, E. Dagotto, and J. Herbrych,
Phys. Rev. B 104, 045128 (2021)
Theoretical analysis of magnetic states of the multiorbital Hubbard ladder in the OSMP is presented, i.e., detailed doping vs. interaction magnetic phase diagram is analyzed. The presented analysis indicates that multiorbital models of iron-based systems combine phenomena known from cuprates (AFM tendencies) with those found in manganites (phase separation) and iron pnictides (block magnetism).

Author contribution: This project was done with my PhD student (I'm the co-supervisor). I initiated the research project. I provided the interpretation of the research results, e.g., I provided the analytical tools necessary for the analysis. I build the hypothesis that more than one Fermi vector is contributing to the magnetic properties of the system. I co-described the magnetic phases. I contributed to the writing of the manuscript. I estimate my contribution to this article to be $\sim 40\%$.

2.3 Description

Introduction

Past experience in Cu-based high-temperature (high-T_c) superconductors (SC) showed that the analysis of the low-dimensional systems, such as chains and ladders, can provide useful information to better contrast theory with the experiments [1–3]. Furthermore, recent advances in cold-atoms in optical lattices [4–11] and also solid-state pump-and-probe experiments challenge our understanding of the out-of-equilibrium situations. As a consequence, accurate results in systems with reduced dimensionality are still of great importance. One reason is that theoretical many-body calculations based on model Hamiltonians can be accurately performed in one dimension (1D), particularly numerically. In this respect, the wave-function-based methods, i.e., exact diagonalization (ED), Lanczos-based algorithms, and density-matrix renormalization group (DMRG) method, allow for unbiased calculations of static and dynamic quantities.

The analysis mentioned above is overwhelmingly done within two paradigmatic models: the single-band Hubbard or Heisenberg Hamiltonians, on various lattices. This stems from the fact that cuprates' normal state (at ambient pressure or at half-electronic-filling) can be described by insulating Mott physics and can be related to its quantum magnetic fluctuations [12, 13]. The inelastic neutron scattering (INS) measurements are crucial for the study of the latter. This powerful experimental technique provides detailed information on momentum- and energy-resolved spin excitations. The importance of INS studies was best illustrated in the early days of high-T_c superconductors [13, 14]. Shortly after discovering the copper-oxide compounds, it became evident that the standard BCS (Bardeen–Cooper–Schrieffer) theory of electron-phonon coupling does not explain the experimental findings. Simultaneously, the INS results showed that superconductivity appears in close proximity to the antiferromagnetic (AFM) ordering of $S = 1/2$ Cu^{2+} moments, providing robust evidence that the new pairing mechanism may be based on spin fluctuations [3]. The latter can be accurately described by the Hubbard model (interacting spinful fermions on a lattice) or, under certain conditions, by the Heisenberg model of interacting spins.

This view has been challenged by the discovery of iron-based (Fe-based) high-T_c superconductors [15–17]. In contrast to the Cu-based materials, which in a normal state are AFM insulators, the Fe-based superconductors are typically "bad metals". Despite this fundamental difference in the parent compounds, the phase diagrams (pressure or electronic filling dependence of T_c) of these materials are qualitatively similar [18–20]. Within the single-band Hubbard phenomenology, large Coulomb interaction U is needed to open an energy gap at the Fermi level. The same interactions also lead to a large magnetic moment $\mathbf{S^2} = S(S+1)$, and AFM ordering observed in Cu-based materials. As a consequence, the metallic state of Fe-based materials questioned the role of magnetic fluctuations (or electronic correlations in general) in the high-T_c superconductivity.

To understand the origin of this paradox, one has to focus on the important difference between Cu and Fe itself, both of which belong to the transition metals. Bulk Cu has filled $3d$ orbitals and one electron on $4s$ band (yielding the charge density close to one electron per site in such materials). On the contrary, bulk Fe has a filled $4s$ band and 6 electrons on five $3d$ orbitals. Consequently, cuprates have a single Fermi surface (FS), which can be accurately described by the single-band Hubbard model. The iron-based compounds have a complicated FS with electron and hole pockets, originating in the five 3d orbitals. This important conceptual difference has to be taken into account during the modeling of Fe-based materials.

The physics of iron superconductors (and materials based on compounds from the pnictogen group) have to be described [17, 21] employing the multiorbital Hubbard model, involving not only the standard Hubbard repulsion but also the Hund coupling. The former describes the interaction of electrons at the same site (orbital), while the latter accounts for Hund's rule: every orbital in a sublevel is singly occupied before any orbital is doubly occupied. Simultaneously, electrons in singly occupied orbitals have the same spin projection and maximize the total spin (the total magnetic moment per site $\mathbf{S}^2$). The generic - SU(2) symmetric - multiorbital Hubbard model is given by:

$$\begin{aligned} H = & - \sum_{\gamma,\gamma',\ell,\sigma} t_{\gamma\gamma'} \left(c^{\dagger}_{\gamma,\ell,\sigma} c_{\gamma',\ell+1,\sigma} + \text{H.c.} \right) + \sum_{\ell,\gamma} \Delta_{\gamma}\, n_{\gamma,\ell} \\ & + U \sum_{\gamma,\ell} n_{\gamma,\ell,\uparrow} n_{\gamma,\ell,\downarrow} + (U - 5J_{\text{H}}/2) \sum_{\gamma<\gamma',\ell} n_{\gamma,\ell} n_{\gamma',\ell} \\ & - 2J_{\text{H}} \sum_{\gamma<\gamma',\ell} \mathbf{S}_{\gamma,\ell} \cdot \mathbf{S}_{\gamma',\ell} + J_{\text{H}} \sum_{\gamma<\gamma',\ell} \left(P^{\dagger}_{\gamma,\ell} P_{\gamma',\ell} + \text{H.c.} \right) , \end{aligned} \tag{1}$$

where $c^{\dagger}_{\gamma,\ell,\sigma}$ creates an electron with spin projection $\sigma = \{\uparrow,\downarrow\}$ at site $\ell = \{1,\ldots,L\}$ of orbital $\gamma = \{0,\ldots,\Gamma-1\}$, with Γ as a number of active orbitals. $t_{\gamma\gamma'}$ and Δ_{γ} denotes a hopping amplitude matrix and the crystal-field splitting in orbital space γ, respectively. The local (γ,ℓ) orbital-resolved particle density is $n_{\gamma,\ell} = \sum_{\sigma} n_{\gamma,\ell,\sigma}$, $\mathbf{S}_{\gamma,\ell}$ is the local spin, and $P_{\gamma,\ell} = c_{\gamma,\ell,\uparrow} c_{\gamma,\ell,\downarrow}$ is the pair-hopping operator. U is the repulsive Hubbard interaction, while J_{H} is the Hund exchange. In the works described here, to reduce the number of parameters in the model, $J_{\text{H}}/U = 1/4$ will be fixed, a value widely used when modeling iron superconductors. Finally, the global filling is given by $n = N/L$, where N is the number of electrons and L is the system size.

The competition between spin, electronic, and orbital degrees of freedom in the above model can lead to novel exotic phases not present in the single-band Hubbard Hamiltonian. A prominent example of a phenomenon unique to multiorbital systems is the so-called orbital-selective Mott phase (OSMP) [22, 23] (see the phase diagram presented in Fig. 1). In general, the single-band Hubbard model in high dimension exhibits a single metal-insulator transition (the Mott-Hubbard transition) as a function of the interaction U (in 1D, the electronic gap has an activated behavior for any finite U). This is in striking contrast to multi-band systems, where competing interactions can lead to the selective localization of electrons on some orbitals - in the same sense as electrons localize within the single-band picture in the large-U limit. Such insulating bands coexist with the metallic band (or bands) with itinerant electrons. It is argued [16] that this unique metal-insulator mixture could be responsible for the bad-metallic behavior of the parent compounds of iron-based superconductors.

It is by now evident that in strongly-correlated systems, both Cu- and Fe-based, high-T_{c} superconductivity is closely connected to a strongly-correlated bad-metal state and/or a nearby AFM order. As such, considerable effort has been devoted to understanding the electron correlation effects and the associated magnetism. In this context, the magnetic properties of the multiorbital system have been much less explored. This stems from a few facts: (*i*) iron-based superconductivity is much younger than its cuprate counterpart. (*ii*) In the single-band Hubbard model, the magnetic moments are not yet fully developed in small U conducting (metallic) phase. As a consequence, in the naive analysis of the bad-metallic state of iron-based materials, the magnetic properties were (often mistakenly) treated as a secondary contribution to overall physics. (*iii*) Lack of reliable methods that can unbiasedly treat the many-body systems, especially the ones with large Hilbert space.

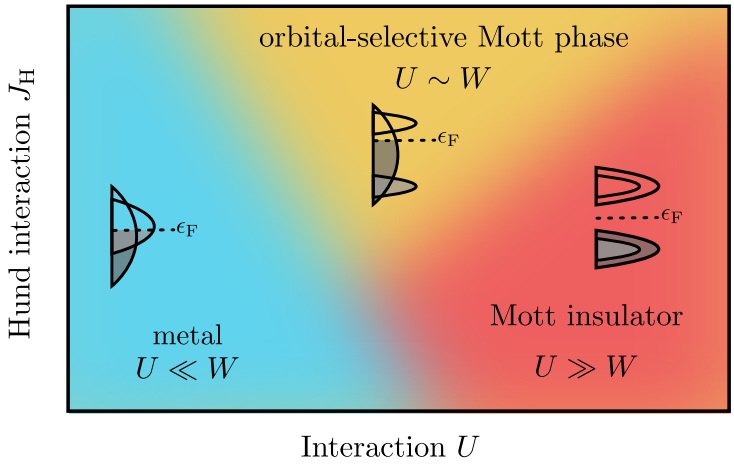

FIGURE 1: Schematic phase diagram of the generic multiorbital Hubbard model. At small $U \ll W$ (with W as the kinetic energy bandwidth), the system is a metal. At large $U \gg W$, the system is in a Mott insulating state. For the intermediate value of interaction strength U and robust value of Hund exchange J_H, the system is in the orbital-selective Mott phase with at least one orbital Mott localized. The schematic shapes of the density-of-states in a given phase are also shown. Figure taken from Ref. [**H4**].

The common goal of the publications submitted as the "scientific achievement" [**H1-H6**] is to describe the magnetism and transport properties of low-dimensional multi-orbital systems, especially in the orbital-selective Mott phase (OSMP). The latter was argued - via angle-resolved photoemission spectroscopy - to be relevant for various two-dimensional iron-based compounds from the 122 family (AFe_2X_2; A-alkali metals, X-chalcogenides), e.g., $(K,Rb)_xFe_2Se_2$ [24] and KFe_2As_2 [25], or in iron-chalcogenides and oxychalcogenides like $FeTe_{1-x}Se_x$ [26] and $La_2O_2Fe_2O(Se,S)_2$ [27]. Furthermore, the low-dimensional materials from the 123 family (quasi-1D ladders AFe_2X_3) exhibit interplay between local moments and delocalized electrons, e.g., $BaFe_2S_3$ and $BaFe_2Se_3$ [23,28–32]. Importantly, the latter can also support the superconducting state [33–37], similarly as it occurs in Cu-based ladders.

Experimental investigations of the magnetic properties of the 123 ladders reported two distinctive magnetic phases. INS on $(Ba,K)Fe_2S_3$ and $(Cs,Rb)Fe_2Se_3$ identified [28, 38–40] ferromagnetic (FM) ordering along the rungs and AFM along the legs, that is, canonical $(\pi, 0)$ order. On the other hand, it was shown [41] that the $BaFe_2Se_3$ compound exhibits exotic spin arrangement of AFM-coupled FM "islands" along the legs, namely $\uparrow\uparrow\downarrow\downarrow$, the so-called block magnetic ordering [$(\pi/2, 0)$ ordering]. The same conclusion was also reached on the basis of neutron [42–44] or X-ray diffraction [44], and muon spin relaxation [44]. Similar magnetic structures were identified in two dimensions in the presence of $\sqrt{5} \times \sqrt{5}$ ordered vacancies $(K,Rb)Fe_2Se_2$ [45–48], in compounds from the family of 245 iron-based SC $(K,Rb)_2Fe_4Se_5$ [49, 50], and also iron-chalcogenides Fe(Se,Te) [51, 52]. Finally, recent first-principles calculations predicted that the block-magnetism may also be relevant for the one-dimensional iron-selenide compound Na_2FeSe_2 [53], iron-oxychalcogenide $Ce_2O_2FeSe_2$ [54], as well as in yet-to-be synthesized iron-based ladder tellurides [55, 56].

The exact-diagonalization of many-body multiorbital systems (1) is destined to fail due to the exponential growth of the Hilbert space of the model: $\dim(H) = 4^{\Gamma L}$ with Γ the number of active orbitals and L the number of sites in the system. To study the physics of such systems, one must rely on some form of approximations. For example, the full five-orbital Hubbard model was investigated via the mean-field Hartree-Fock analysis [57–

59], revealing a complex filling-Hund/Hubbard interaction magnetic phase diagram with many competing phases. Many of such phases were also confirmed by density functional theory [36,37,55,56,59–61]. Moreover, the electronic properties of the multiorbital Hubbard model were extensively investigated via the dynamical mean-field theory [16,22,62].

The aforementioned theoretical approaches are limited because they cannot properly incorporate the effects of quantum fluctuations over long distances. This issue is particularly important for the low-dimensional systems (e.g., relevant for 123 family of Fe-based ladders), where it is well known that quantum fluctuations must be treated accurately, thereby requiring the full many-body calculations. In order to facilitate the latter, an alternative route has to be taken, such as decreasing the number of considered orbitals. For instance, it was shown [21] that the three-orbital Hubbard model could accurately describe the physics of iron-based materials. In the latter, the e_g orbitals ($d_{x^2-y^2}$ and d_{z^2}) are far enough from the Fermi level to be neglected, rendering only the t_{2g} orbitals (d_{xy}, d_{xz}, d_{yz}) active. Accordingly, one has to decrease the number of considered electrons. The octahedral splitting present in the iron ladders of the 123 family leads to the so-called high-spin state (maximal spin projection) with 2 electrons in the e_g orbitals. Consequently, 4 electrons on three t_{2g} orbitals seem to be the minimal model to describe the iron-based systems. Nevertheless, despite these approximations, accurate many-body simulations of three-orbital systems are mostly restricted to the chain geometry and static quantities, with ladders and dynamical quantities (frequency/energy-dependent) being largely out of reach.

As already discussed, the multiorbital Hubbard model requires a considerable numerical effort to be accurately described. The results discussed in the following were obtained using the zero-temperature $T = 0$ density matrix renormalization group (DMRG) method with a single-center site approach [63–66]. The dynamical correlation functions were calculated using the dynamical-DMRG method [67–69], evaluated directly in terms of frequency via the Krylov decomposition [69, 70]. Furthermore, all results were obtained for the generic values of kinetic parameters of the model (1), i.e., coexisting wide and narrow energy bands in $U \to 0$ limit (as suggested by the DFT calculations for 123 materials [21, 71]). For the three- $\Gamma = 3$ and two-orbital $\Gamma = 2$ Hubbard model, the hopping amplitude matrix was given by

$$t_{\gamma\gamma'} = \begin{pmatrix} -0.50 & 0.00 & 0.10 \\ 0.00 & -0.50 & 0.10 \\ 0.10 & 0.10 & -0.15 \end{pmatrix}, \qquad t_{\gamma\gamma'} = \begin{pmatrix} -0.50 & 0.00 \\ 0.00 & -0.15 \end{pmatrix}, \tag{2}$$

and the crystal-field splitting $\Delta_0 = -0.1$, $\Delta_1 = 0.0$, $\Delta_2 = 0.8$ and $\Delta_0 = 0.0$, $\Delta_1 = 0.8$, respectively.

Static spin properties

The magnetic properties of quantum systems are usually investigated via the static structure factor $S(q)$, i.e., by the Fourier transform of real-space spin-spin correlation function

$$S(q) = \frac{1}{L} \sum_{\ell,m} \mathrm{e}^{-\imath q(\ell-m)} \langle \mathbf{S}_\ell \cdot \mathbf{S}_m \rangle , \tag{3}$$

with L as the system size (the 1D chain of L sites) and wavevector (momentum) $q = 2\pi m/L$ with $m = 0, \ldots, L-1$. Note that $\mathbf{S}_\ell = \sum_\gamma \mathbf{S}_{\gamma,\ell}$ represents the total on-site spin. For the canonical AFM ordering, the maximum of the structure factor $S(q)$ is at $q_{\max} = \pi$ wavevector (for FM ordering it is at $q_{\max} = 0$). The analysis of the 1D three-orbital Hubbard model within OSMP has shown [71] that already for moderate interaction strength

$U \sim J_{\mathrm{H}} \sim W$ (where W is a kinetic energy of the system) - and electronic filling $n = 4/3$ - the system develops the block-magnetic ordering (the $\uparrow\uparrow\downarrow\downarrow\uparrow\uparrow\downarrow\downarrow$ spin arrangement) with $q_{\mathrm{max}} = \pi/2$. Interestingly, this result was later confirmed [41] by the INS spectrum of the $BaFe_2Se_3$ powder.

Within the aforementioned setup, one of the orbitals is fully localized with $n_2 = 1$, and two others are itinerant with $n_0 \simeq n_1 \simeq 1.5$ (yielding 4 electrons in total). In Ref. **[H2]**, we further simplify the model by neglecting one of the itinerant orbitals (together with decreasing the overall filling by 1.5 electrons per site). The premise for the two-orbital model relies on the fact that d_{yz}- and d_{xz}-orbitals are often close to being degenerate in AFe_2X_3 materials. Such a result is consistent with crystal-field theory predictions for, e.g., $BaFe_2Se_3$ [41]. The octahedral splitting in the latter (ligands being pulled from the central atom in the unit cell) can give rise to two approximately degenerated bands and one higher in energy orbital. The 1D model used in the analysis of magnetism of iron chains and ladders [21,71] indeed captures such behavior, as evident from, e.g., equal occupation of two out of three of the orbitals. Interestingly, the analysis of the two-orbital model, i.e., the dependence of occupations on the interaction U and filling n, presented in Ref. **[H2]** reveals an effective Hamiltonian of the OSMP.

In Ref. **[H2]**, it was argued that the two-orbital Hubbard model with electron density above half-filling always exhibits OSMP due to the crystal field splitting $\Delta_1 = 0.8\,[\mathrm{eV}]$ (as suggested by the DFT considerations of the 123 family of iron-based materials). As a consequence, in a broad range of the electronic filling $2 < n < 3$, the system has one localized band with $n_1 = 1$ and one itinerant (metallic) orbital with fractional filling $1 < n_0 < 2$ (with $n = n_0 + n_1$). Note that for $U > W$ and at $n = 2$ (half-filling), the system is in the Mott state with AFM ordering and $\mathbf{S}^2 = S(S+1) = 2$. On the other hand, at $n = 3$, the system is a mixture of the Mott insulator with $n_1 = 1$ and band insulator with $n_0 = 2$, with AFM ordering and $\mathbf{S}^2 = 3/4$. For intermediate $2 < n < 3$, the $\mathbf{S}^2$ is also maximized to a value dependent on the specific choice of n. The saturated $\mathbf{S}^2$, single electron occupation of n_1, vanishing charge fluctuations $\delta n_\gamma^2 = \langle n_\gamma^2 \rangle - \langle n_\gamma \rangle^2$ on $\gamma = 1$ orbital, flat momentum distribution function $n(q)$ of $\gamma = 1$, and the gap in the orbital resolved spectral function $A(q, \omega)$ of $\gamma = 1$ electrons (see also discussion later on) indicate that the system is in the orbital-selective phase. Furthermore, the aforementioned behavior of the localized orbital $\gamma = 1$ indicates that doublons and holons don't contribute to the low-energy physics and can be traced out by standard Schrieffer-Wolff transformation [72] [restricted to $\gamma = 1$ orbital of (1)]. As a consequence, in Ref. **[H2]** it was shown that the effective model of the OSMP can be written in the form of generalized Kondo-Heisenberg (gKH) Hamiltonian

$$\begin{aligned} H_{\mathrm{K}} = & - t_{00} \sum_{\ell,\sigma} \left(c^\dagger_{0,\ell,\sigma} c_{0,\ell+1,\sigma} + \mathrm{H.c.} \right) + U \sum_{\ell} n_{0,\ell,\uparrow} n_{0,\ell,\downarrow} \\ & + K \sum_{\ell} \mathbf{S}_{1,\ell} \cdot \mathbf{S}_{1,\ell+1} - 2J_{\mathrm{H}} \sum_{\ell} \mathbf{S}_{0,\ell} \cdot \mathbf{S}_{1,\ell} \,. \end{aligned} \tag{4}$$

The first two terms of the model describe the mobile electrons of the itinerant $\gamma = 0$ band. The third term describes the behavior of the spins $\mathbf{S}_{1,\ell}$ of the localized $\gamma = 1$ electrons with spin exchange given by $K = 4t_{11}^2/U$. Finally, the last term is the Hund coupling between spins at different orbitals. Note that the electronic filling of the effective Hamiltonian is either $n_{\mathrm{K}} = n - 1$ or $n_{\mathrm{K}} = 3 - n$, due to the particle-hole symmetry of (4).

The accuracy of H_{K} was tested on various static and dynamical quantities: (*i*) in Ref. **[H2]** the static structure factor $S(q)$ was compared with the results obtained with the help of the full two-orbital Hamiltonian. (*ii*) In Ref. **[H3]**, the single-particle spectral

function $A(q,\omega)$ was also compared with the latter. (*iii*) In Ref. [**H4**], the dynamical structure factor $S(q,\omega)$ was compared with the two-orbital and three-orbital results obtained in Ref. [**H1**]. Perfect agreement with the effective Hamiltonian has been found for all considered quantities. Furthermore, because of the restricted (smaller) Hilbert space of (4), more accurate results could be reached.

In Fig. 2(a) a direct comparison of the static structure factor $S(q)$ between (1) with $\Gamma = 2$ and (4) for $U/W = 1$ is presented (with $W = 2.1$ [eV]). As expected, for $n = 2$ ($n_{\rm K} = 1$), the system exhibits AFM ordering with $q_{\rm max} = \pi$, i.e., $\uparrow\downarrow\uparrow\downarrow$ alternating correlations [also presented in the top panel of Fig. 2(a)]. Upon electron doping, for $n = 2.5$ ($n_{\rm K} = 0.5$) the $q_{\rm max} = \pi/2$ block magnetism $\uparrow\uparrow\downarrow\downarrow\uparrow\uparrow\downarrow\downarrow$ is stabilized. Note that these results agree with the three-orbital consideration [71], due to the orbital degeneracy in that model ($n = n_0 + n_1 + n_2 = 1.5 + 1.5 + 1$). In addition, in Ref. [**H2**] new types of block magnetism have been revealed. For electronic filling $n = 2.66$ ($n_{\rm K} = 0.33$), the $q_{\rm max} = \pi/3$ ordering of $\uparrow\uparrow\uparrow\downarrow\downarrow\downarrow\uparrow\uparrow\uparrow\downarrow\downarrow\downarrow$-form can be found. Finally, due to the larger system sizes L numerically available for (4), the block-magnetism of four spins with $q_{\rm max} = \pi/4$ at $n_{\rm K} = 0.25$ was found.

The tendencies for block formation within OSMP can be understood from the limits of the gKH model (4):

(*i*) for $t_{00} \gg (U\,, J_{\rm H})$: the system is in the paramagnetic (PM) state, with short-range features in $S(q)$ at $q = 2k_{\rm F}$ (the so-called Fermi instability), where $k_{\rm F}$ is a Fermi vector given by the electronic filling $2k_{\rm F} = \pi n_{\rm K}$ (for the chain lattice geometry in $U \to 0$ limit),

(*ii*) for $J_{\rm H} \gg (t_{00}\,, U)$: the itinerant electrons form local triplets with localized spins (due to the FM Hund exchange),

(*iii*) for $J_{\rm H} \sim t_{00} \gg U$: increasing mobility of the electrons leads to a double-exchange FM ordering known from the Kondo-like modes [73],

(*iv*) for $J_{\rm H} \sim U \sim W$: the Hubbard interaction U promotes AFM ordering, and the latter competes with FM ordering due to the double exchange mechanism. Consequently, the system minimizes its energy by forming FM islands that are AFM coupled. In other words: the interaction U "stabilizes Fermi instability" and promotes $q_{\rm max} = 2k_{\rm F}$ as a quasi-long-range order.

Note that the exotic block-magnetic patterns found in chains and ladders (described in Ref. [**H2**] and Ref. [**H5**], respectively) are not static as would be the case for a combination of domain walls or a spin density wave, but exhibit significant quantum fluctuations with local $\langle S^z_\ell \rangle = 0$. For example, in the case of the block pattern $\uparrow\uparrow\downarrow\downarrow$, Lanczos diagonalization studies presented in Ref. [**H1**] confirm that the many-body ground-state is in at least 50% of the singlet form

$$|\uparrow\uparrow\downarrow\downarrow\rangle - |\downarrow\downarrow\uparrow\uparrow\rangle\,.$$

Accordingly, individual magnetic blocks should be considered as regions with strong FM correlations, as opposed to domains with finite magnetization.

The generalized Kondo-Heisenberg model allowed for a detailed analysis of $S(q)$ for various parameters. Fig. 2(b) depicts one of the main findings of Ref. [**H2**], i.e., interaction U - filling n magnetic phase diagram of the OSMP in 1D. At $U < W$, the ground-state is a paramagnetic metal. For $U \gtrsim W$ the system enters OSMP with coexisting metallic and Mott-insulating bands. For sufficiently large values of interaction $U \gg W$ the system is in a FM state for all fillings [consistent with $J_{\rm H} \gg t_{00}$ prediction of point (*iii*) above].

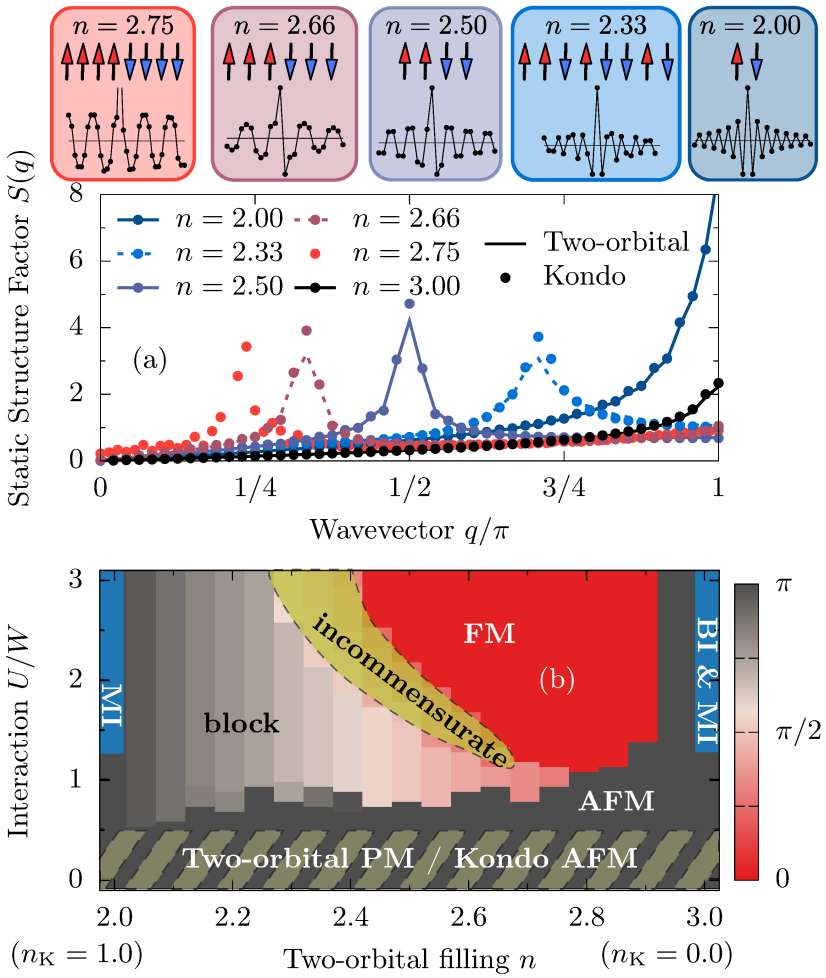

FIGURE 2: (a) Static structure factor $S(q)$ for various fillings n at fixed $U = W$, for two-orbital Hubbard (lines) and generalized Kondo-Heisenberg (points) models. Real-space correlation functions $\langle \mathbf{S}_\ell \cdot \mathbf{S}_{L/2} \rangle$ and sketches of the spin alignment are also presented at the top. (b) Interaction U vs. filling n magnetic phase diagram of the generalized Kondo-Heisenberg model. The dashed-shaded area represents the region where the mapping is not valid. Figure taken from Ref. **[H2]**.

When $U \sim \mathcal{O}(W)$, namely when all energy scales compete, the system is in the block-magnetic state. Depending on the filling of the itinerant band n_K, the spins form various sizes of AFM-coupled FM spin islands. That is, we have explicitly checked that $q_{\max}(n)$ follows the $2k_F$ obtained as the maximum of $\mathrm{d}n(q)/\mathrm{d}q$, i.e., by the inflection point of the momentum distribution function. Interestingly, this prediction is also valid for the three-orbital Hubbard model and also for the ladder geometry (as discussed later on and in Ref. **[H5]**).

The initial investigation presented in Ref. **[H2]** identified an incommensurate order between block and FM phase (see Fig. 2b). More detailed analysis of this region in Ref. **[H3]** revealed another exotic magnetic ordering. Additional information about the magnetic properties can be obtained from the so-called chirality correlation function $\widetilde{\kappa}^d(|\ell - m|) = \langle \kappa^d_\ell \cdot \kappa^d_m \rangle$, where

$$\kappa^d_\ell = \mathbf{S}_\ell \times \mathbf{S}_{\ell+d} \,. \tag{5}$$

It is evident that the above expectation is always zero for AFM, FM, and block ordering since the spins are always parallel or antiparallel.

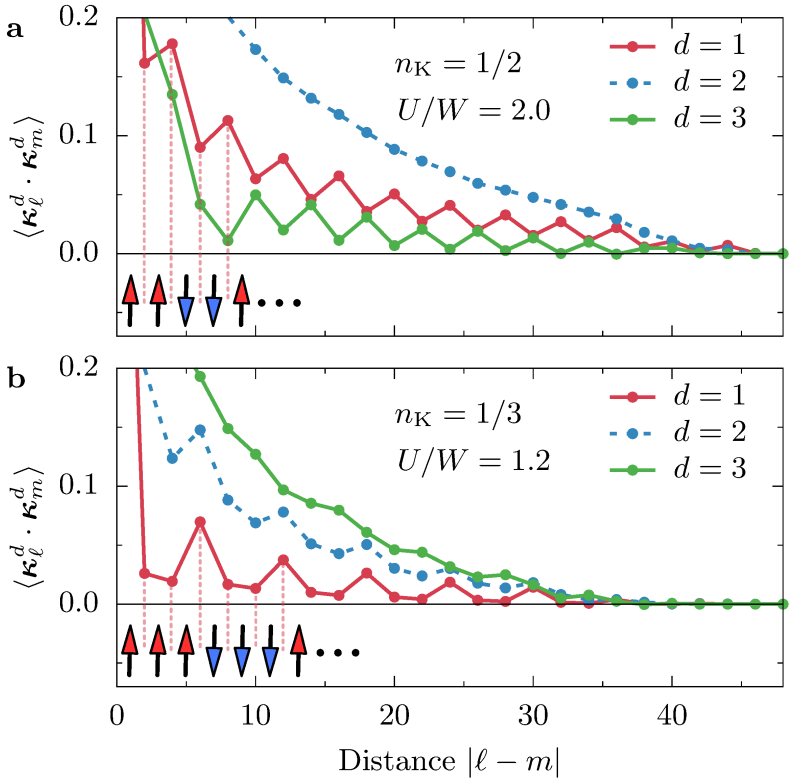

FIGURE 3: (**a**) Dependence of the chiral correlation function $\langle \kappa_\ell^d \cdot \kappa_m^d \rangle$ ($\kappa_\ell^d = \mathbf{S}_\ell \times \mathbf{S}_{\ell+d}$) on distance d between spins. Results were calculated using the generalized Kondo-Heisenberg model with $n_K = 0.5$ and $U/W = 2.0$. Panel (**b**): same as (**a**) but for $n_K = 0.33$ and $U/W = 1.2$. In both panels: arrows represent schematics of the block order for given filling. Figure taken from Ref. [**H3**].

Interestingly, in the region (initially) marked as incommensurate, the $\langle \kappa_\ell^d \cdot \kappa_m^d \rangle$ correlation has finite value and strongly depends on the choice of distance d, as evident from the results presented in Fig. 3. The former indicates that the spins have a spiral ordering, with some angle of rotation θ. Furthermore, the spatial structure of $\langle \kappa_\ell^1 \cdot \kappa_m^1 \rangle$ displays a clear zig-zag-like pattern for the nearest-neighbour ($d = 1$) spins. To better investigate the spiral internal structure, Fig. 3 depicts the dependence of the chirality correlation on the distance d. Specifically, for $n_K = 0.5$ ($n_K = 0.33$) the correlation function oscillates every two (three) sites. Interestingly, these patterns change their nature when the next–nearest neighbour ($d = 2$) chirality is considered: (*i*) the values of these chiralities increase $\langle \kappa_\ell^2 \cdot \kappa_m^2 \rangle > \langle \kappa_\ell^1 \cdot \kappa_m^1 \rangle$, and (*ii*) for the case of $n_K = 0.5$ the κ-correlation is now a smooth function of distance, while $n_K = 0.33$ still exhibits some three-site oscillations. Investigating the next-next–nearest neighbour case, $d = 3$, provides additional information. While for the $n_K = 0.5$ filling the $d = 3$ correlations are smaller than $d = 1$ and $d = 2$, for $n_K = 0.33$ they are larger and (as for $d = 2$ at $n_K = 0.5$) they are now a smooth function of distance.

This seemingly erratic behavior of $\langle \kappa_\ell^d \cdot \kappa_m^d \rangle$ correlations varying d cannot be simply explained by a mere uniform change of the pitch angle θ of the spiral magnetic order. To better explain this behavior, let us focus on the dimer correlation defined [74] as

$$D_{\pi/2} = \frac{2}{L} \sum_{\ell=L/4}^{3L/4} (-1)^{\ell-1} \langle \mathbf{S}_\ell \cdot \mathbf{S}_{\ell+1} \rangle \,. \tag{6}$$

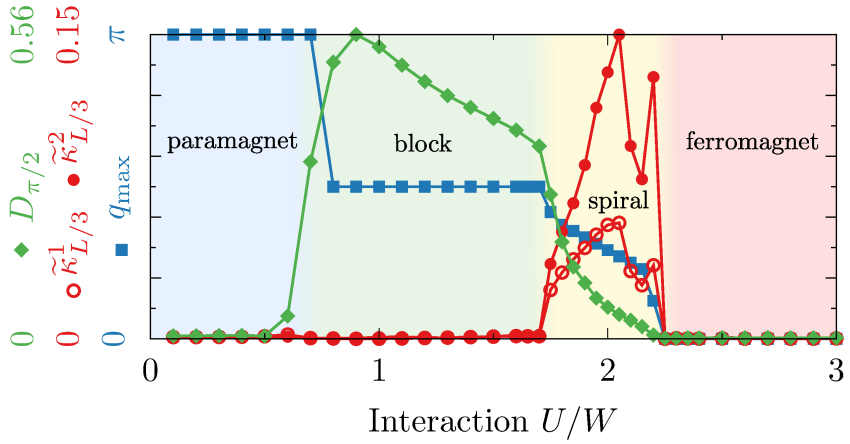

FIGURE 4: Phase diagram varying the interaction U/W. Presented are: (*i*) maximum of the static spin structure factor $q_{\max}$ (squares), (*ii*) nearest–($d = 1$) and next–nearest ($d = 2$) neighbour chirality $\widetilde{\kappa}^d_{L/3}$ (open and filled circles, respectively), and (*iii*) dimer correlation $D_{\pi/2}$ (diamonds). Results were calculated using the generalized Kondo-Heisenberg model for $n_{\rm K} = 0.5$. Figure taken from Ref. **[H3]**.

The above quantity compares the number of FM and AFM bonds in the bulk system. For true FM or AFM ordered states, each nearest–neighbour bond has the same sign: positive for FM ↑↑ and negative for AFM ↑↓. Consequently, $D_{\pi/2} = 0$. On the other hand, in the $\pi/2$-block state ↑↑↓↓ the FM and AFM bonds alter in a staggered fashion rendering $D_{\pi/2} \neq 0$. Fig. 4 depicts the interaction U dependence of $D_{\pi/2}$ for $n_{\rm K} = 0.5$. Furthermore, in the same figure, the wavevector $q_{\max}$ for which the static structure factor $S(q)$ is maximized, and the value of the $\widetilde{\kappa}^d_{L/3}$ correlator for $d = 1$ and $d = 2$ is shown. Starting in the paramagnet at small U, both $D_{\pi/2}$ and $\widetilde{\kappa}^d_{L/3}$ vanish, with $q_{\max} = \pi$ depicting the usual short-range staggered correlations of weak-U physics. In the opposite limit of the strong interaction, $U \gg W$, $D_{\pi/2} = \widetilde{\kappa}^d_{L/3} = 0$ as well, the consequence of a simple FM state with $q_{\max} = 0$. In the most exciting case of competing interaction $U \sim W$, the dimer correlation $D_{\pi/2}$ acquires a finite value maximized at $U \simeq W$. The latter reflects a perfect $\pi/2$-block magnetic state. Interestingly, one can observe a continuous transition of $D_{\pi/2}$ between the block and FM phases in the region where a finite chirality $\widetilde{\kappa}^d_{L/3} \neq 0$ was found and where $q_{\max}$ takes incommensurate values.

Based on the above results, Ref. **[H3]** presents a coherent picture explaining the nature of the magnetic state between the block and FM phases. Consider first filling $n_{\rm K} = 0.5$. At $U \simeq W$ the ground-state is a block–magnetic phase, where two-site FM islands (blocks) are AFM coupled. Increasing the interaction U, the spins start to rotate w.r.t. each other, inducing finite $\langle \kappa^d_\ell \cdot \kappa^d_m \rangle$ correlations. Remarkably, during the rotation, the overall FM-islands nature of the state is preserved, yielding a finite $D_{\pi/2} \neq 0$ all the way to the FM state at $U \gg W$. Such an unexpected scenario is also encoded in the inequalities $\widetilde{\kappa}^2_{L/3} > \widetilde{\kappa}^1_{L/3}$ and $\widetilde{\kappa}^2_{L/3} > \widetilde{\kappa}^3_{L/3}$ observed in Fig. 3(a). This is qualitatively different from a standard spiral state, where the spin rotates from site-to-site. For the case discussed in Ref. **[H3]**, the spiral is made out of individual blocks, and it is the entire block that rotates from block-to-block (see Fig. 5). This new spiral state is stabilized without any apparent frustration, the common avenue to generate spiral arrangements in, e.g., multiferroics. The same arguments can be used for $\pi/3$ blocks ↑↑↑↓↓↓ and $d = 3$ chirality correlation.

Works Ref. **[H2]** and Ref. **[H3]** discussed the magnetic properties of the orbital-selective Mott insulators on the chain geometry. Since the 123 family of iron-based materials are

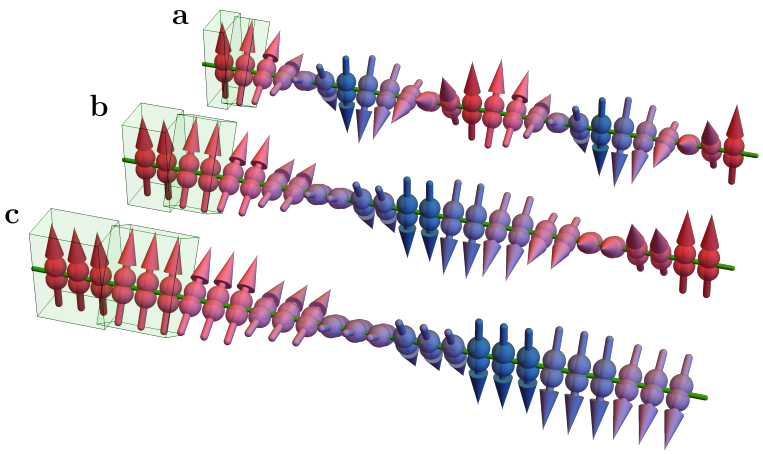

FIGURE 5: Schematic representation of spirals within the orbital-selective Mott phase. Top to Bottom: (a) standard spiral magnetic structure with site-to-site spins rotation and (b,c) block–spirals of two and three sites, respectively.

quasi-1D (they are ladders with significant inter-chain hopping exchange), Ref. [**H6**] contains a comprehensive analysis of the magnetic phases within the OSMP of multiorbital Hubbard ladders. The results are summarized in Fig. 6. As already discussed, the shape and size of the block-magnetism is related to the electronic density via the Fermi vector. Since the ladders can (in principle) have more than one Fermi point, one can expect a more complicated phase diagram. For two-leg ladder geometry, a symmetrical and antisymmetrical energy bands are allowed, resulting from a symmetrical or antisymmetrical linear combination of the wave function on the rungs of the ladder (in the one-particle basis). At large fillings, $n_K \gtrsim 1.6$, where the antibonding band is fully filled and only

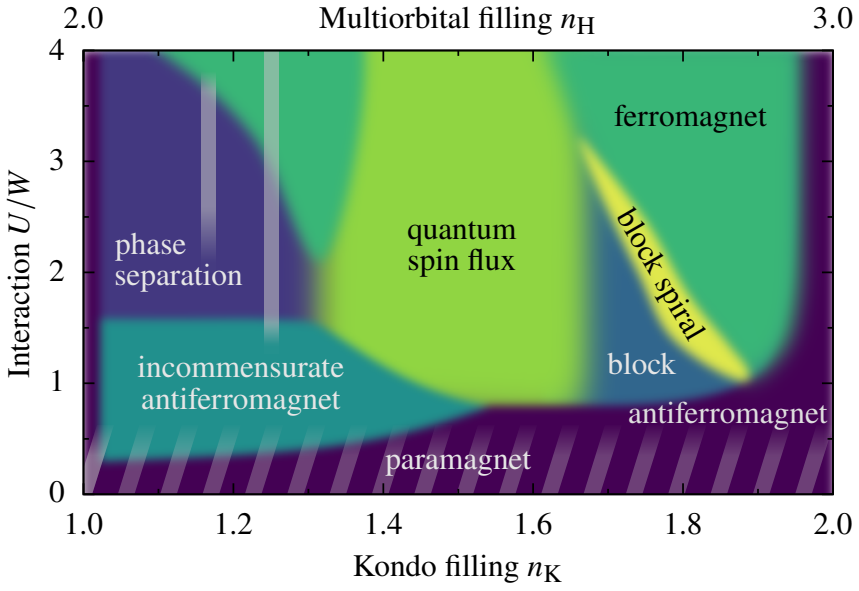

FIGURE 6: Schematic U-n_K magnetic phase diagram of the generalized Kondo-Heisenberg ladder. The vertical lines within the phase-separation regime mark special fillings $n_K = 1.17, 1.25$, where perfect block orders are recovered. Figure taken from Ref. [**H6**].

the bonding band carries the Fermi wavevectors, the system develops perfect blocks of $\begin{smallmatrix}\uparrow\uparrow\\ \uparrow\uparrow\end{smallmatrix}\begin{smallmatrix}\downarrow\downarrow\\ \downarrow\downarrow\end{smallmatrix}$-form at $U \sim W$. Increasing the strength of the interaction U leads to the uniform rotation of the blocks, i.e., to the formation of the exotic block-spiral phase (similarly as it was the case on the chain geometry). In the opposite limit, close to half-filling $n_{\mathrm{K}} \sim 1$, the two Fermi wavevectors present in two bands drive the system towards phase separation with (predominantly) π, $\pi/2$, and $\pi/3$ blocks. Finally, when $n_{\mathrm{K}} \sim 1.5$, the ladder system develops a quantum spin flux originating in the competing energy scales inherent to the OSMP. This phase can be naively viewed as staggered spin currents circulating within 2×2 plaquettes (however, no plaquette carries net current due to its quantum nature). In summary, the analysis presented in Ref. **[H6]** indicates that the magnetic phase diagram of iron ladders is dominated by tendencies to form magnetic blocks of various shapes and sizes. Furthermore, the phase diagram contains the phases known from cuprates (AFM tendencies) with those found in manganites (phase separation) and iron pnictides (block magnetism).

Dynamical spin properties

Up to now, we have discussed the zero-temperature static properties of the multiorbital Hubbard model and the effective model of the OSMP, i.e., the ground-state magnetic ordering. It is also instructive to focus on the momentum-resolved excitations. The INS experiment on the $BaFe_2Se_3$ ladder [41] (exhibiting the block $\uparrow\uparrow\downarrow\downarrow$ magnetism) revealed the existence of low-energy acoustic and high-energy optical modes separated by an energy gap. Similar findings were obtained for $BaFe_2S_3$ [40], and $RbFe_2Se_3$ [39], albeit the plain canonical $(\pi, 0)$ ordering was identified in those compounds. Since the measurements were performed on the powder samples, no detailed information on the momentum dependence within the Brillouin zone was given (due to the spherical momentum averaging).

Ref. **[H1]** presents the first (to the authors' knowledge) numerical study of the dynamical spin structure factor (SSF) $S(q,\omega)$ of a multiorbital Hubbard model. The zero-temperature spin dynamics can be obtained from the dynamical correlation function

$$S(q,\omega) = -\frac{1}{L\pi}\sum_{\ell=1}^{L} \mathrm{e}^{-iq(\ell-L/2)}\,\mathrm{Im}\,\langle \mathrm{GS}|\widetilde{\mathbf{S}}_{\ell}\,\frac{1}{\omega^{+}-H+\epsilon_0}\,\widetilde{\mathbf{S}}_{L/2}|\mathrm{GS}\rangle\,, \tag{7}$$

where $\omega^{+} = \omega + i\eta$ with η as a broadening, and $|\mathrm{GS}\rangle$ as the ground-state with energy ϵ_0. In the above equation $\widetilde{\mathbf{S}}_{\ell} = \sum_{\gamma} \mathbf{S}_{\ell,\gamma}$ is the total spin on-site ℓ for the total $S(q,\omega)$, or $\widetilde{\mathbf{S}}_{\ell} = \mathbf{S}_{\ell,\gamma}$ for the orbital resolved dynamical spectra $S_{\gamma\gamma'}(q,\omega)$.

Fig. 7 contains one of the main results of Ref. **[H1]**: the frequency-momentum dependence of the dynamical SSF in the block-OSMP phase (i.e., at $U/W = 0.8$ with $W = 2.45\,[\mathrm{eV}]$) within three-orbital $\Gamma = 3$ Hubbard model (1). Panel (a) depicts the total SSF, $S(q,\omega)$, while panel (b) shows only the contribution from the localized orbital, $S_{22}(q,\omega)$. Several conclusions can be obtained directly from the presented results: (*i*) A robust contribution to the total SSF arises from the localized orbital. Moreover, all the qualitative features of $S(q,\omega)$ are already present in $S_{22}(q,\omega)$. In fact, $S(q,\omega)$ and $S_{22}(q,\omega)$ become almost indistinguishable if normalized by the local magnetic moment squared (i.e., $\mathbf{S}^2 = 3/4$ for the $S = 1/2$ localized electron, and $\mathbf{S}^2 = 2$ for the total moment for the three-orbital system). (*ii*) The energy range for the spin dynamics is much smaller when compared with the energy bandwidth $W = 2.45\,[\mathrm{eV}]$ of the Hamiltonian. (*iii*) Clearly, the dynamical SSF has two distinct modes: a low-frequency, $\omega \lesssim \omega_c = 0.08\,[\mathrm{eV}]$, dispersive (acoustic) band and a high-frequency, $\omega \sim 0.11\,[\mathrm{eV}]$, dispersionless (optical) band. The latter mode resembles the previously reported high-energy features of $BaFe_2Se_3$ [41]

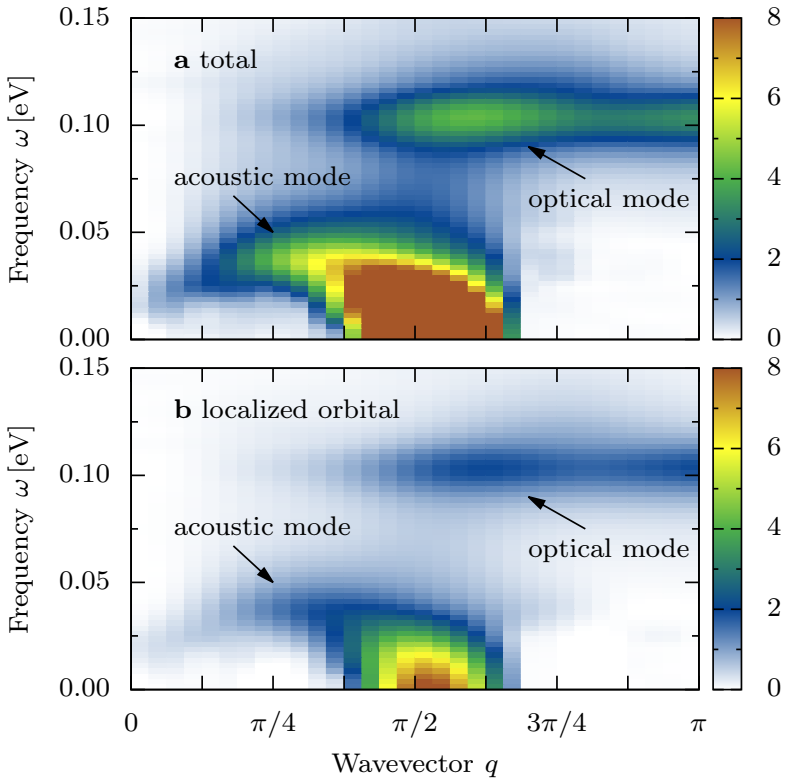

FIGURE 7: (a) Total dynamical spin structure factor $S(q,\omega)$, and (b) of the localized orbital, $S_{22}(q,\omega)$. The results were obtained on the three-orbital Hubbard model for $n = 4/3$. Figure taken from Ref. [**H1**].

(with 2×2 FM blocks), and $BaFe_2S_3$ [40] or $RbFe_2Se_3$ [39] (with $(\pi, 0)$ order, which can be viewed as 2×1 FM blocks). The different types of blocks in the INS investigations, and the similarity of the results between neutrons and model calculations, suggest that the results of Ref. [**H1**] apply to a wide variety of iron chalcogenides. The arguments presented in Ref. [**H1**] and also in Ref. [**H4**] indicate that the low-energy mode is dominated by the spin excitations between the magnetic blocks (with the blocks acting as a rigid unit) spanning in momentum space between zero and the propagation wavevector $q_{\max}$ of the magnetic unit cell (of the block). On the other hand, the optical mode is attributed to local excitations inside the block (or even within one site) controlled by the on-site Hund exchange.

Motivated by the results presented above, with the main contribution to the SSF arising from the localized orbital, one can express the eigenstates in terms of the basis states of localized orbital $|\cdot\rangle_{\gamma=2}$. Since in the OSMP the electrons are localized with occupation $n_{\gamma=2} = 1$ [71], in the low-energy portion of the spectrum the basis states with empty and doubly occupied orbital $\gamma = 2$ should not be present [as argued in Ref. [**H2**] via the effective model (4)]. Within such a representation, the ground-state of the block-OSMP phase can be identified as a superposition of $|\uparrow\uparrow\downarrow\downarrow\rangle_{\gamma=2}$ and $|\downarrow\downarrow\uparrow\uparrow\rangle_{\gamma=2}$ states which constitutes $\sim 50\%$ of the true ground-state. One can improve further the qualitative description by investigating a simple toy model. Let us consider two FM coupled $S = 1/2$ spins as one $S = 1$ object, i.e., $|\mathbf{1}\rangle = |\uparrow\uparrow\rangle_{\gamma=2}$, $|-\mathbf{1}\rangle = |\downarrow\downarrow\rangle_{\gamma=2}$, and $|\mathbf{0}\rangle = 1/\sqrt{2}(|\uparrow\downarrow\rangle_{\gamma=2} + |\uparrow\downarrow\rangle_{\gamma=2})$. In this setup, a 4-site $S = 1/2$ system reduces to two antiferromagnetically coupled $S = 1$

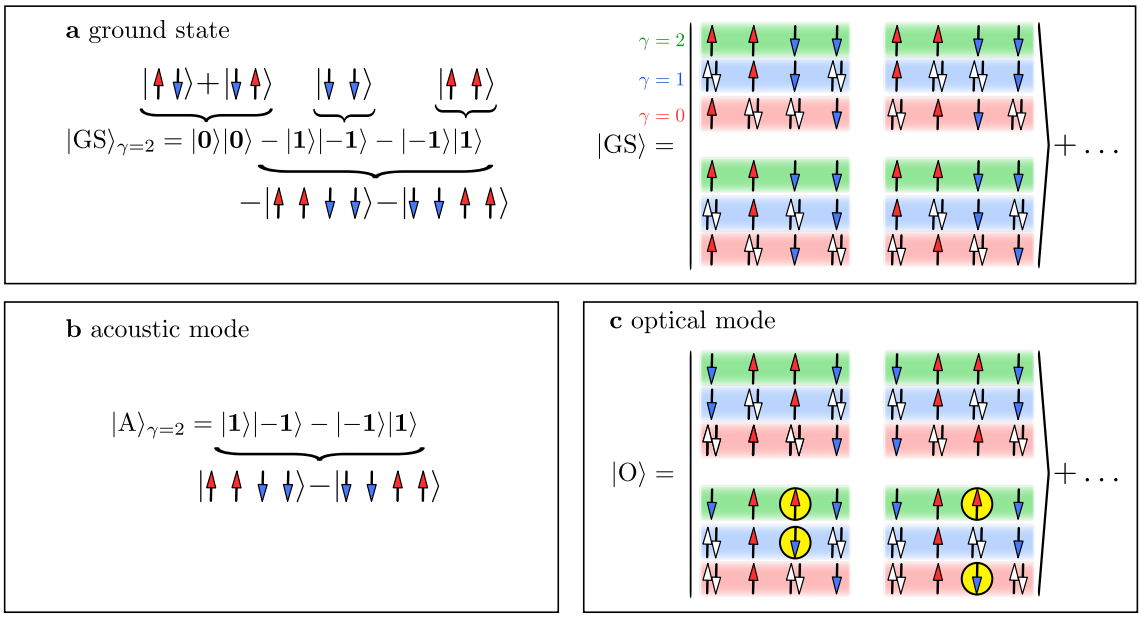

FIGURE 8: Spin configuration in the localized orbital ($\gamma = 2$) of the (a) ground-state $|\mathrm{GS}\rangle$ (singlet) and (b) excited state $|\mathrm{A}\rangle$ (triplet) contributing to the acoustic mode within three-orbital Hubbard model. (c) Schematic representation of the particle configuration of all orbitals of the $|\mathrm{GS}\rangle$ and optical triplet $|\mathrm{O}\rangle$. Circles represent pairs of antiferromagnetically aligned spins that break Hund's rule. Figure taken from Ref. [**H1**].

spins. The ground-state of the latter is simply

$$|\mathrm{GS}\rangle_{\gamma=2} = c_a|\mathbf{0}\rangle|\mathbf{0}\rangle - c_b\Big(|\mathbf{1}\rangle|-\mathbf{1}\rangle - |-\mathbf{1}\rangle|\mathbf{1}\rangle\Big)\,, \tag{8}$$

where $c_a = c_b = 1/\sqrt{3}$ [see Fig. 8(a) for a schematic representation]. Note that the above state, in agreement with numerics, is a singlet. The last two terms of Eq. (8) correspond to the "perfect" block order, i.e., $|\uparrow\uparrow\downarrow\downarrow\rangle_{\gamma=2}$ and $|\downarrow\downarrow\uparrow\uparrow\rangle_{\gamma=2}$, while the first term depicts the x–y component of the block order,

$$|\mathbf{0}\rangle|\mathbf{0}\rangle = \frac{1}{2}\Big(|\uparrow\downarrow\uparrow\downarrow\rangle_{\gamma=2} + |\downarrow\uparrow\downarrow\uparrow\rangle_{\gamma=2} + |\uparrow\downarrow\downarrow\uparrow\rangle_{\gamma=2} + |\downarrow\uparrow\uparrow\downarrow\rangle_{\gamma=2}\Big)\,. \tag{9}$$

Lanczos investigation of the $L = 4$ site $\Gamma = 3$ system (1) indicates that the state (8) has coefficients equal to $c_a^2 \simeq 1/6$ and $c_b^2 \simeq 1/4$, which yields now a better overlap, $\sim 70\%$, with the true ground-state. Finally, the first excited state - contributing to the acoustic mode - can be identified as a triplet of the form

$$|\mathrm{A}\rangle_{\gamma=2} = c_A(|\uparrow\uparrow\downarrow\downarrow\rangle_{\gamma=2} + |\downarrow\downarrow\uparrow\uparrow\rangle_{\gamma=2})\,, \tag{10}$$

where $c_A^2 \simeq 4/9$ [see Fig. 8(b)]. The toy model also captures this large overlap of $|\mathrm{A}\rangle_{\gamma=2}$ with the full solution since $|\mathbf{1}\rangle|-\mathbf{1}\rangle - |-\mathbf{1}\rangle|\mathbf{1}\rangle$ is one of the first excitations in our two-site $S = 1$ problem.

To properly understand the optical mode, it is not enough to focus solely on the localized orbital. Instead, one has to focus on the full three-orbital representation of the state. Lanczos analysis presented in Ref. [**H1**] indicates that the high-energy mode arises from a state of the form

$$|\mathrm{O}\rangle_{\gamma=2} \simeq 1/2(|\downarrow\uparrow\uparrow\downarrow\rangle_{\gamma=2} + |\uparrow\downarrow\downarrow\uparrow\rangle_{\gamma=2})\,. \tag{11}$$

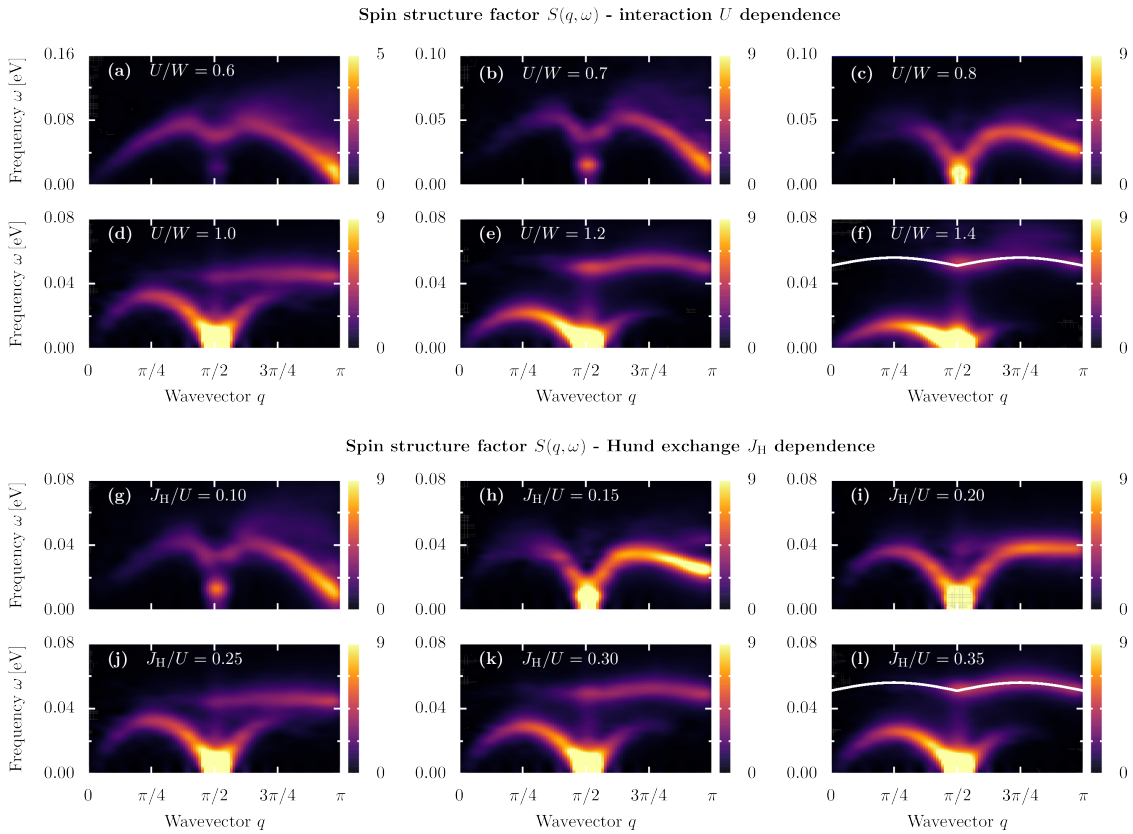

FIGURE 9: (a-f) Hubbard U and (g-l) Hund exchange J_H dependence of the dynamical spin structure factor $S(q,\omega)$, calculated for generalized Kondo-Heisenberg model for $n_K = 0.5$. Panels (a-f) show results for $U/W = 0.6,\ldots,1.4$ and $J_H/U = 0.25$, while panels (g-l) for $J_H = 0.1,\ldots,0.35$ and $U/W = 1$. The white line in panels (f) and (l) indicate the $\omega_O(q) = 0.051 + 0.005|\sin(2q)|$ dispersion. Figure taken from Ref. **[H4]**.

A detailed analysis of the remaining "metallic" orbitals $\gamma = 0, 1$ indicates that: (*i*) the $|GS\rangle$ and the $|A\rangle$ states obey Hund's rule: spins in different orbitals of the same site are ferromagnetically aligned [see Fig. 8(a)]. (*ii*) However, the $|O\rangle$ states, Fig. 8(c), do not fulfill this rule since part of the spins are antiferromagnetically aligned. As a consequence, the main difference in energy between the $|GS\rangle$ and $|O\rangle$ arises from the local (on-site) Hund exchange portion of the electronic interaction.

Similarly as in the case of static properties, the effective Hamiltonian of the OSMP, i.e., the generalized Kondo-Heisenberg model (4), allows for a more detailed analysis of the dynamical spin structure factor $S(q,\omega)$. The results of Ref. **[H4]** contain a comprehensive study - interaction U and Hund exchange J_H dependence - of the spin dynamics within OSMP. The main findings are summarized in Fig. 9. Note that, at weak interaction, $U \to 0$, the gKH model does not accurately describe multiorbital physics because of the assumption of having spin localization in one of the orbitals. Ref. **[H2]** indicates that the mapping is valid for $U/W \gtrsim 0.5$.

At small U, the system is in the paramagnetic state and the dynamical spin structure factor $S(q,\omega)$ resembles the $U \to 0$ result of the single-band Hubbard model at given filling n_K. Increasing the interaction U and entering the block-phase at $U \sim W$, the spin

spectrum changes drastically [see Figs. 9(a-d)]. Firstly, the spectral weight of the low-energy dispersive mode shifts from the wavevectors range $\pi/2 < q < \pi$ to the region around $q \simeq \pi/2$ (for general filling the spectral weight accumulates at $q \simeq 2k_{\rm F}$). This weight transfer reflects the emergence of the block-magnetic order $\uparrow\uparrow\downarrow\downarrow$ at propagation wavevector $q_{\rm max} = 2k_{\rm F}$. Consequently, in the block-OSMP, the low-energy short-wavelength $q > \pi/2$ spin excitations are highly suppressed. This indicates that at low energy the spin excitations within the magnetic unit cell (within the magnetic island) cannot occur, and the spectrum is thus dominated by excitations between different blocks.

The second characteristic feature upon increasing the interaction U is the high-frequency, seemingly momentum-independent, optical mode. As shown in Fig. 9(c-d), for $U \sim U_{\rm c} \simeq 0.8W$ - concurrently to the shift of the weight previously described - the dispersion $\omega(q)$ of the spin excitations is heavily modified in the short-wavelength limit. Namely, increasing the interaction up to $U \sim U_{\rm c}$ increases and flattens the $\omega(\pi/2 < q < \pi)$ features. It is interesting to note that the results of the static structure factor $S(q)$ presented in Ref. **[H2]** indicate that the system enters the block-OSMP at $U \simeq U_{\rm c}$. For $U > U_{\rm c}$ the flat band "detaches" from the dispersive portion of $\omega(q)$ and creates a novel momentum-independent mode $\omega_{\rm O}$. Increasing the interaction strength U/W further leads to the increase of the frequency where this optical mode is observed [see Figs. 9(d-f)]. At the same time, the energy span of the acoustic mode $\omega_{\rm A}(q)$ decreases. The latter qualitatively resembles the usual behavior of spin superexchange in the Mott limit, i.e., $J \propto 1/U$.

Interestingly, in the block OSMP, the dispersive mode $\omega_{\rm A}(q)$ is weakly dependent on $J_{\rm H}$, opposite to the behavior of the optical mode, as shown in Fig. 9(g-l). Such behavior is consistent with the analysis given in Ref. **[H1]**, i.e., that the localized spin excitations $\omega_{\rm O}$ are predominantly controlled by the local Hund exchange $J_{\rm H}$. Finally, Ref. **[H4]** shows that for large $J_{\rm H}$ the optical band develops a narrow sine-like dispersion. This is depicted in Fig. 9(f) (for $U = 1.4\,W$ and $J_{\rm H} = 0.25\,U$) and in Fig. 9(l) ($U = W$ and $J_{\rm H} = 0.35\,U$). Although the energy range of the acoustic mode changes (due to varying U), it is clear that the optical bands behave similarly for both parameter sets. The latter can be described with a simple fit $\omega_{\rm O}(q) = \omega_0 + \widetilde{J}_{\rm O}\sin(q/2)$, with ω_0 as the frequency offset and $\widetilde{J}_{\rm O} = 0.005\,[\text{eV}]$ providing a very small dispersion. This indicates that the excitations contributing to the optical mode can propagate within the magnetic unit cell (within a magnetic island) for large values of the Hund exchange.

Electronic properties

Another interesting aspect is the electron excitations within the OSMP. Since the latter is in an overall metallic state, one can expect a finite weight at the Fermi level $\epsilon_{\rm F}$ in the density-of-states (DOS). In Ref. **[H3]** and Ref. **[H5]**, we have addressed this issue, i.e., we studied the effect of block and block-spiral magnetism on the single-particle spectral function $A(q,\omega) = A^{\rm e}(q,\omega) + A^{\rm h}(q,\omega)$. The latter is defined as

$$A^{\rm e}(q,\omega) = -\frac{1}{L\pi}\sum_{\ell} {\rm e}^{-iq(\ell-L/2)}\,{\rm Im}\langle {\rm GS}|c^{\dagger}_{\gamma,\ell}\frac{1}{\omega^{+}-H+\epsilon_0}c_{\gamma,L/2}|{\rm GS}\rangle\,, \qquad (12)$$

$$A^{\rm h}(q,\omega) = -\frac{1}{L\pi}\sum_{\ell} {\rm e}^{-iq(\ell-L/2)}\,{\rm Im}\langle {\rm GS}|c_{\gamma,\ell}\frac{1}{\omega^{+}+H-\epsilon_0}c^{\dagger}_{\gamma,L/2}|{\rm GS}\rangle\,, \qquad (13)$$

where $c_{\gamma,\ell} = c_{\gamma,\ell,\uparrow} + c_{\gamma,\ell,\downarrow}$. $A^{\rm e}(q,\omega)$ [$A^{\rm h}(q,\omega)$] represents retarded (electron photoemission) and advanced (hole inverse–photoemission) part of the spectrum, respectively. The density-of-states can be calculated as ${\rm DOS}(\omega) = 1/(\pi L)\sum_q A(q,\omega)$ and similarly for the electron and hole parts. Note that $A(q,\omega)$ is directly relevant for the angle-resolved photoemission spectroscopy.

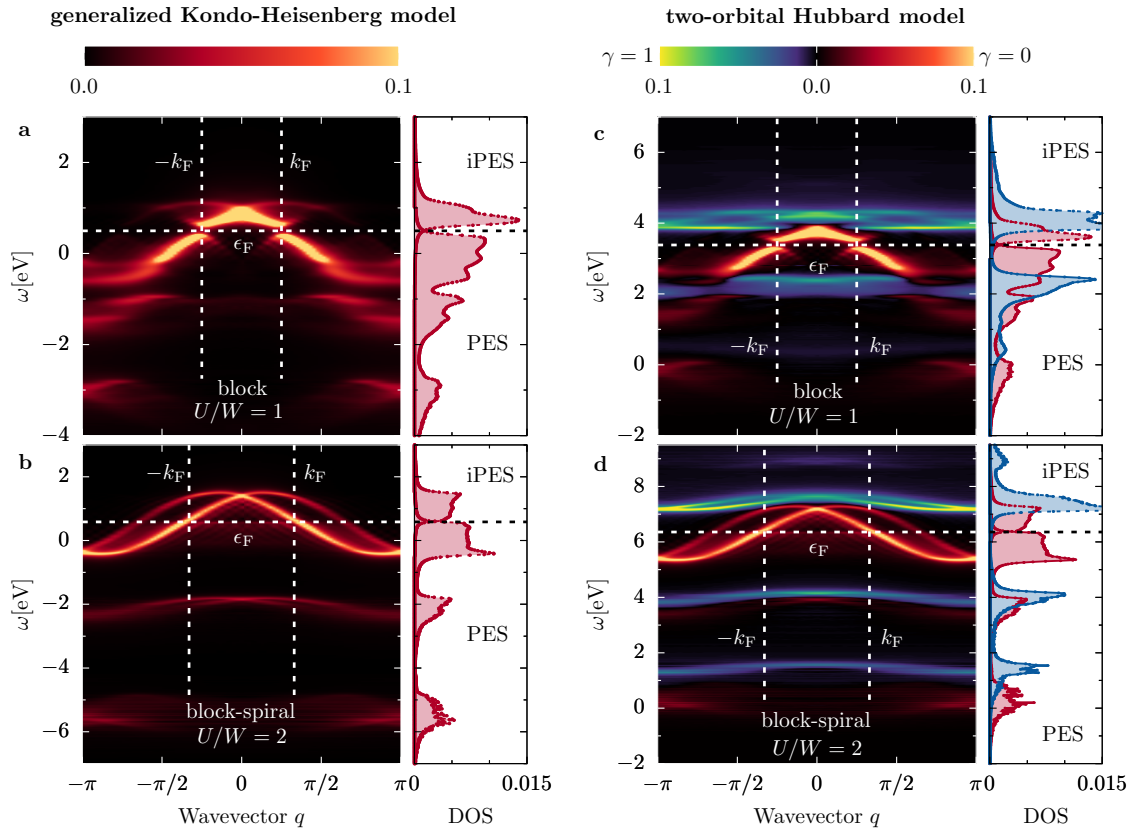

FIGURE 10: Spectral function $A(q,\omega)$ of (a) block-phase ($n_K = 1.5\,, U/W = 1.0$) and (b) block-spiral-phase ($n_K = 1.5\,, U/W = 2.0$) as calculated for the generalized Kondo-Heisenberg model. (c,d) The same results obtained with the two-orbital Hubbard model: (c) block-phase ($n = 2.5\,, U/W = 1.0$) and (d) block-spiral-phase ($n = 2.5\,, U/W = 2.0$). Horizontal (vertical) lines depict the Fermi level ϵ_F (Fermi wavevector k_F), while (i)PES stands for (inverse-) photoemission spectroscopy. Right panels: density-of-states $\mathrm{DOS}(\omega) = 1/(\pi L)\sum_q A(q,\omega)$. Figure taken from Ref. [**H3**].

As already discussed, a distinctive feature of the OSMP is the coexistence of localized electrons (spins in an insulating band) and itinerant electrons (a metallic band). In the block-magnetic phase at $U \simeq W$ it was previously shown [31] – for the three-orbital Hubbard model – that the density-of-states (DOS) at the Fermi level ϵ_F is reduced, indicating a pseudogap-like behavior. Ref. **[H3]** provides the analysis of $A(q,\omega)$ and $\mathrm{DOS}(\omega)$ for the two-orbital Hubbard model (1) and the gKH model (4), see Fig. 10. Such a comparison can also serve as a nontrivial test of the strength of our OSMP effective Hamiltonian. Specifically, the results presented in Fig. 10 indicate that the behavior of the gKH model, Fig. 10(a,b), perfectly matches the $\gamma = 0$ itinerant orbital of the full two-orbital Hubbard result presented in Fig. 10(c,d). Furthermore, the flat in momentum space bands of $\gamma = 1$ orbital are in agreement with Mott electron localization. Finally, the spectral gap in $\gamma = 1$ orbital further supports the arguments for the gKH effective model. Also, it is important to note that although the system is overall metallic in nature, the band structure is vastly different from the simple cosine-like result of $U \to 0$. The distinctive features in $A(q,\omega)$ at the Fermi vector k_F, and a large renormalization of the overall band structure at higher energies indicate a complex interplay between various degrees of freedom and energy scales.

When the interaction U increases and the systems enter the block-spiral region, the

single-particle spectral function $A(q,\omega)$ changes drastically. In Fig. 10(b) we show representative results for the pitch angle $\theta/\pi \simeq 0.3$ block-spiral state at $U/W = 2$ and $n_K = 1.5$. Two conclusions are directly evident from the presented results: (*i*) the pseudogap at ϵ_F is closed, but some additional gaps at higher energies opened. (*ii*) $A(q,\omega)$ in the vicinity of the Fermi level, $\omega \sim \epsilon_F$, develops two bands, intersecting at the $q = 0$ and $q = \pi$ points, with the maximum at $q \simeq \theta/2$. The analysis presented in Ref. [**H3**] showed that the bands represent two quasiparticles: left- and right-movers reflecting the two possible rotations of the spirals. It is obvious from the above results that the quasiparticles break the parity symmetry, i.e., going from $q \to -q$ momentum changes the quasiparticle character, as expected for a spiral state. Somewhat surprisingly, $A(q,\omega)$ does not show any gap as would typically be associated with the finite dimerization $D_{\pi/2}$ that we observe. However, it should be noted that for quantum localized $S = 1/2$ spins the quarter-filling ($n_K = 1.5$) implies a filling of $2/5$ of the lower Kondo band (due to the energy difference between local Kondo singlets and triplets). The dimerization gap expected at $\pi/2$ would thus open away from the Fermi level and would not confer substantial energy gain to the electrons. Thus, it was concluded that the quantum fluctuations of the localized and itinerant spins are strong enough to suppress the dimerization gap. The above conclusions can also be reached from results obtained with the full two-orbital Hubbard model [see Figs. 10(d)].

The parity-breaking quasiparticles discussed in Ref. [**H3**] resemble the ones found in the single-orbital Hubbard model with spin-orbit coupling (SOC) [75]. Such a particle dispersion is an essential ingredient, together with the SC gap, in some of the candidate setups [76, 77] for the Majorana zero-energy modes (MZM). However, the large spin-orbit coupling required to split the doubly-degenerated bands due to the electronic spins renders such a setup hard to engineer. In Ref. [**H5**], we have shown that the many competing energy scales induced by the correlation effects present in superconducting multiorbital systems lead to a topological phase transition and the appearance of MZM. Unlike the other proposed MZM candidate setups, our scheme does not require frozen classical magnetic moments or, equivalently, FM ordering in the presence of the Rashba spin-orbit coupling [78]. All ingredients necessary to host Majorana modes appear as a consequence of the quantum effects induced by the electron-electron interaction within the OSMP (as described above and in Ref. [**H3**]).

To show that an OSMP-like system can support MZM in Ref. [**H5**] we have studied

$$H_{SC} = H_K + \Delta_{SC} \sum_{\ell} \left(c^{\dagger}_{\ell,\uparrow} c^{\dagger}_{\ell,\downarrow} + \text{H.c.} \right), \tag{14}$$

where Δ_{SC} is an on-site singlet SC pairing amplitude. The latter can be induced by the proximity effect with a BCS superconductor, or it could be an intrinsic property of the iron superconductors under pressure or doping. It is important to note that the coexistence of SC and nontrivial magnetic properties is mostly impossible in single-orbital systems. Here, the OSMP provides a unique platform in which this constraint is lifted by, on the one hand, spatially separating such phenomena and, on the other hand, strongly correlating them with each other.

Figure 11 shows the effect of $\Delta_{SC}/W \simeq 0.5$ on the single-particle spectral function $A(q,\omega)$ for the two crucial phases in our study, the block- and block-spiral magnetic orders ($U/W = 1$ and $U/W = 2$, respectively). As expected, in both cases, a finite superconducting gap opens at the Fermi level ϵ_F (~ 0.5 [eV] for $U/W = 1$ and ~ 0.1 [eV] for $U/W = 2$). Remarkably, an additional prominent feature appears in the block-spiral phase: a sharply localized mode inside the gap at ϵ_F, displayed in Fig. 11(b). Such an in-gap mode is a characteristic feature of a topological state, namely, the bulk of the system

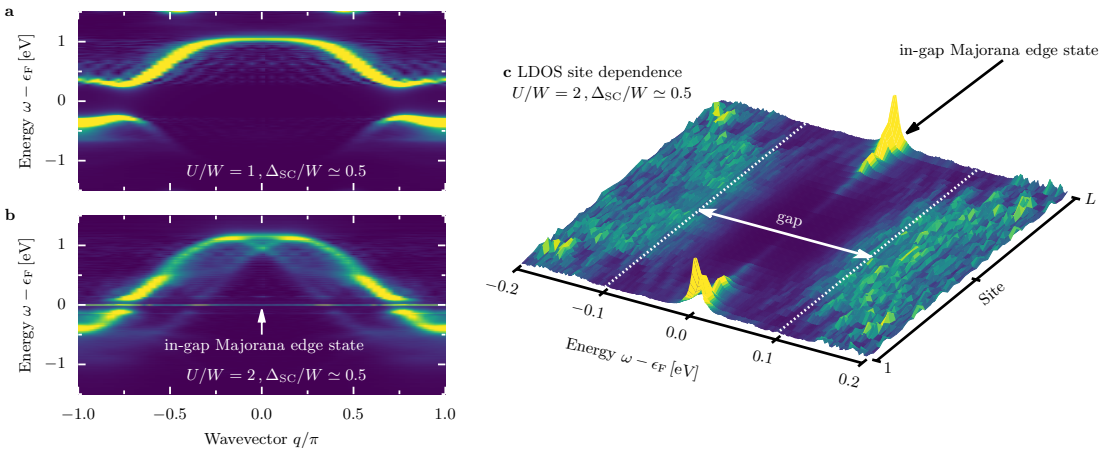

FIGURE 11: (a) Effect of the finite pairing field $\Delta_{SC}/W \simeq 0.5$ on the single-particle spectral function $A(q,\omega)$ for (a) $U/W = 1$ and (b) $U/W = 2$ calculated within generalized Kondo-Heisenberg model for $n_K = 0.5$. Majorana zero-energy modes are indicated in (b). (c) Local density-of-states (LDOS) in the in-gap frequency region vs. chain site index. The sharp LDOS peaks at the edges represent Majorana edge states, while the bulk of the system exhibits gapped behavior. Figure taken from Ref. [**H5**].

is gapped, whereas the edge of the system contains the in-gap modes. To confirm this picture, in Fig. 11(c), we present high-resolution frequency data of the real-space local density-of-states (LDOS) near the Fermi energy ϵ_F. As expected, for a topologically non-trivial phase, the zero-energy modes are indeed confined to the system's edges. It is important to note that this phenomenon is absent for the weaker interaction $U/W = 1$. Furthermore, one cannot deduce this behavior from the $U \to \infty$ or $J_H \to \infty$ limits, where the system has predominantly collinear AFM or FM ordering, leading again to a trivial superconducting behavior. However, at moderate U the competing energy scales present in the OSMP lead to the topological phase transition controlled by the electron-electron interaction.

Let's discuss the phase diagram of MZM. Fig. 12 depicts the Hubbard U interaction dependence of the edge-LDOS ($\ell = 1$) in the vicinity of the Fermi level, $\omega \sim \epsilon_F$. It is evident from the presented results that the edge-LDOS acquires a finite value quite abruptly for $U > U_c^T \simeq 1.5$. The same figure depicts the chirality correlation function $\langle \kappa^1_{L/2} \cdot \kappa^1_\ell \rangle$. One can observe a sudden appearance of the chirality correlation exactly at U_c^T, a behavior similar to that of the edge LDOS. Interestingly, in the system without the pairing field (discussed above and in Ref. [**H3**]), at a similar value of $U \simeq 1.6$ the block-spiral phase is stabilized with rigidly rotating FM islands. Furthermore, since the MZMs at the edges of the system are mutually correlated in a finite system, one should detect the sudden increase of the entanglement. The latter can be measured by the von Neumann entanglement entropy $S_{vN}(\ell) = -\mathrm{Tr}\rho_\ell \ln \rho_\ell$ (here ρ_ℓ is a reduced density matrix of the subsystem of the size ℓ). Results presented in Fig. 12 for the system divided into two halves, $\ell = L/2$, indeed indicate that this is the case.

The above results indicate that the system undergoes a topological phase transition upon increasing the strength of the Hubbard interaction U within the OSMP with SC pairing field. The transition is driven by the change in the magnetic properties of the system, namely by inducing a finite chirality visible in the $\langle \kappa^1_\ell \cdot \kappa^1_m \rangle$ correlation function. Furthermore, the results presented in Ref. [**H5**] are consistent with the appearance of the MZM

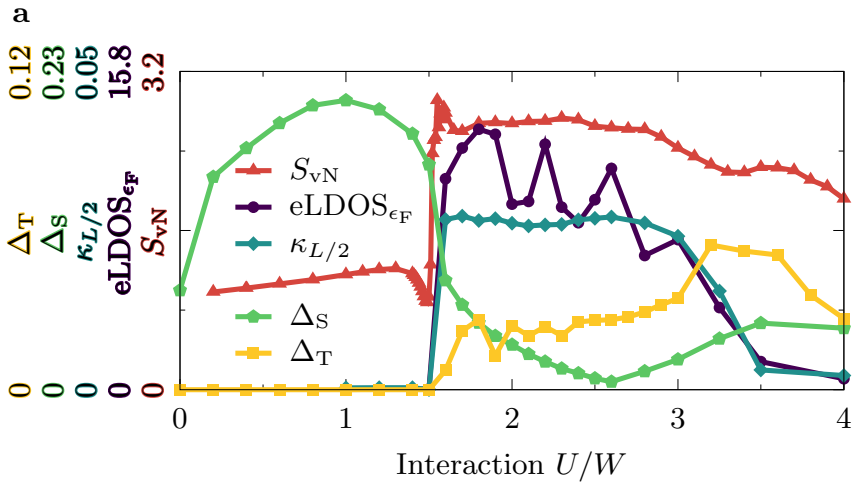

FIGURE 12: Hubbard interaction U dependence of the (*i*) von Neumann entanglement entropy S_{vN}, (*ii*) edge local density-of-states at the Fermi level (eLDOS$_{\epsilon_{\mathrm{F}}}$), (*iii*) the value of chirality correlation function at a distance $L/2$ [i.e., $\widetilde{\kappa}^1(L/2)$], as well as (*iv*) nonlocal singlet Δ_{S} and triplet Δ_{T} pairing amplitudes. Results were obtained with the help of the generalized Kondo-Heisenberg model for $n_{\mathrm{K}} = 0.5$ and $\Delta_{\mathrm{SC}}/W = 0.5$. Figure taken from Ref. [**H5**].

at the topological transition. It should be noted that the presence of MZM implies unconventional triplet superconductivity [77]. The latter is an emergent phenomenon that we also found in our setup. In Fig. 12, we present nonlocal singlet and triplet superconducting amplitudes in the function of the interaction U. That is, we present singlet Δ_{S} and triplet Δ_{T} amplitudes, respectively, defined as

$$\Delta_{\mathrm{S}} = \sum_{\ell=L/4}^{3L/4} |\Delta_{\mathrm{S},\ell}| \,, \qquad \Delta_{\mathrm{T}} = \sum_{\ell=L/4}^{3L/4} \left(|\Delta_{\mathrm{T0},\ell}| + \left|\Delta_{\mathrm{T}\downarrow,\ell}\right| + \left|\Delta_{\mathrm{T}\downarrow,\ell}\right| \right) , \tag{15}$$

with

$$\begin{aligned} \Delta_{\mathrm{S},\ell} &= \left\langle c^{\dagger}_{\ell,\uparrow} c^{\dagger}_{\ell+1,\downarrow} - c^{\dagger}_{\ell,\downarrow} c^{\dagger}_{\ell+1,\uparrow} \right\rangle , \qquad \Delta_{\mathrm{T0},\ell} = \left\langle c^{\dagger}_{\ell,\uparrow} c^{\dagger}_{\ell+1,\downarrow} + c^{\dagger}_{\ell,\downarrow} c^{\dagger}_{\ell+1,\uparrow} \right\rangle , \\ \Delta_{\mathrm{T}\uparrow,\ell} &= \left\langle c^{\dagger}_{\ell,\uparrow} c^{\dagger}_{\ell+1,\uparrow} \right\rangle , \quad \Delta_{\mathrm{T}\downarrow,\ell} = \left\langle c^{\dagger}_{\ell,\downarrow} c^{\dagger}_{\ell+1,\downarrow} \right\rangle . \end{aligned} \tag{16}$$

In view of the above results, the following rationale could explain the origin of topological properties within iron-based materials [79–83]: the competing energy scales present in multiorbital compounds, induced by changes in the Hubbard interaction due to chemical substitution or pressure, lead to exotic magnetic spin textures. Together with the superconducting tendencies, the latter lead to a topologically nontrivial phases exhibiting the MZM.

Conclusions

To summarize, the orbital-selective Mott phase is an emergent phenomenon of strongly-correlated systems with multiorbital Fermi surface, i.e., it originates from the competition between spin, electron, and orbital degrees of freedom. Series of publications [**H1-H6**] revealed novel phenomena significantly different from the one observed in cuprates (described by single orbital Hubbard model).

The most prominent feature of the OSMP is the tendency to form a magnetic blocks of various shapes and sizes, depending on filling and lattice geometry. The observed spin structures are related to the Fermi vector $2k_F$ of the metallic electron bands, but spin blocks are much more sharply defined than they would be in the mere sinusoidal structure arising from a weak-coupling Fermi-surface instability. The strongly correlated nature of the localized spins, due to its narrow bandwidth, enhances the $2k_F$ instability in a manner only possible in the OSMP regime.

The excitations within OSMP also reveal features unique to the multiorbital systems. The analysis presented above indicates that the spin spectra exhibit two modes: (*i*) the acoustic mode associated with the dynamics of spin blocks and (*ii*) the optical band which arises from the on-site inter-orbital spin fluctuations controlled by the Hund exchange coupling. Furthermore, the OSMP displays exotic behavior in the electronic degrees of freedom due to the coexistence of metallic and insulating bands. As shown above, the electron-electron interactions drive the system into the state with parity breaking quasiparticles and even to a nontrivial topological state with Majorana modes.

The effective model of the OSMP described above, i.e., the generalized Kondo-Heisenberg model, allows for a more detailed study of such physics. Also, the results described here provide motivation and theoretical guidance for crystal growers and experimentalists to discover new iron-based chain and ladder compounds that may display the highly unusual properties reported above.

Bibliography

[1] E. Dagotto, Rev. Mod. Phys. **66**, 763 (1994).

[2] E. Dagotto and T. M. Rice, Science **271**, 618 (1996).

[3] D. J. Scalapino, Rev. Mod. Phys. **84**, 1383 (2012).

[4] R. Jördens, N. Strohmaier, K. Günter, H. Moritz, and T. Esslinger, Nature **455**, 204 (2008).

[5] U. Schneider, L. Hackermüller, S. Will, Th. Best, I. Bloch, T. A. Costi, R. W. Helmes, D. Rasch, and A. Rosch, Science **322**, 1520 (2008).

[6] J. V. Porto, Science **340**, 1297 (2013).

[7] R. A. Hart, P. M. Duarte, T.-L. Yang, X. Liu, T. Paiva, E. Khatami, R. T. Scalettar, N. Trivedi, D. A. Huse, and R. G. Hulet, Nature **519**, 211 (2015).

[8] P. T. Brown, D. Mitra, E. Guardado-Sanchez, R. Nourafkan, A. Reymbaut, C.-D. Hébert, S. Bergeron, A.-M. S. Tremblay, J. Kokalj, D. A. Huse, P. Schauß, and W. S. Bakr, Science **363**, 379 (2019).

[9] J. Koepsell, J. Vijayan, P. Sompet, F. Grusdt, T. A. Hilker, E. Demler, G. Salomon, I. Bloch, and C. Gross, Nature **572**, 358 (2019).

[10] P. T. Brown, E. Guardado-Sanchez, B. M. Spar, E. W. Huang, T. P. Devereaux, and W. S. Bakr, Nat. Phys. **16**, 26 (2019).

[11] J. Vijayan, P. Sompet, G. Salomon, J. Koepsell, S. Hirthe, A. Bohrdt, F. Grusdt, I. Bloch, and C. Gross, Science **367**, 186 (2020).

[12] P. A. Lee, N. Nagaosa, and X.-G. Wen, Rev. Mod. Phys. **78**, 17 (2006).

[13] J. M. Tranquada, G. Xu, and I. A. Zaliznyak, J. Magn. Magn. Mater **350**, 148 (2014).

[14] J. M. Tranquada, *Handbook of High-Temperature Superconductivity: Neutron Scattering Studies of Antiferromagnetic Correlations in Cuprates*, Springer New York (2007).

[15] G. R. Stewart, Rev. Mod. Phys. **83**, 1589 (2011).

[16] A. Georges, L.d. Medici, and J. Mravlje, Annu. Rev. Condens. Matter Phys. **4**, 137 (2013).

[17] R. M. Fernandes and A. V. Chubukov, Rep. Prog. Phys. **80**, 014503 (2017).

[18] M. Uehara, T. Nagata, J. Akimitsu, H. Takahashi, N. Mori, and K. Kinoshita, J. Phys. Soc. Jpn. **65**, 2764 (1996).

[19] D. N. Basov and A. V. Chubukov, Nat. Phys. **7**, 272 (2011).

[20] M. J. P. Gingras and P. A. McClarty, Rep. Prog. Phys. **77**, 056501 (2014).

[21] M. Daghofer, A. Nicholson, A. Moreo, and E. Dagotto, Phys. Rev. B **81**, 014511 (2010).

[22] L. de' Medici, S. R. Hassan, M. Capone, and X. Dai, Phys. Rev. Lett. **102**, 126401 (2009).

[23] J. M. Caron, J. R. Neilson, D. C. Miller, K. Arpino, A. Llobet, and T. M. McQueen, Phys. Rev. B **85**, 180405(R) (2012).

[24] M. Yi, D. H. Lu, R. Yu, S. C. Riggs, J.-H. Chu, B. Lv, Z. K. Liu, M. Lu, Y.-T. Cui, M. Hashimoto, S.-K. Mo, Z. Hussain, C. W. Chu, I. R. Fisher, Q. Si, and Z.-X. Shen, Phys. Rev. Lett. **110**, 067003 (2013).

[25] F. Hardy, A. E. Bohmer, D. Aoki, P. Burger, T. Wolf, P. Schweiss, R. Heid, P. Adelmann, Y. X. Yao, G. Kotliar, J. Schmalian, C. Meingast, Phys. Rev. Lett. **111**, 027002 (2013).

[26] M. Yi, Z.-K. Liu, Y. Zhang, R. Yu, J.-X. Zhu, J. J. Lee, R. G. Moore, F. T. Schmitt, W. Li, S. C. Riggs, J.-H. Chu, B. Lv, J. Hu, M. Hashimoto, S.-K. Mo, Z. Hussain, Z.Q. Mao, C. W. Chu, I. R. Fisher, Q. Si, Z.-X. Shen and D. H. Lu, Nat. Comm. **6**, 7777 (2014).

[27] J.-X. Zhu, R. Yu, H. Wang, L. L. Zhao, M. D. Jones, J. Dai, E. Abrahams, E. Morosan, M. Fang, and Q. Si, Phys. Rev. Lett. **104**, 216405 (2010).

[28] S. Chi, Y. Uwatoko, H. Cao, Y. Hirata, K. Hashizume, T. Aoyama, and K. Ohgushi, Phys. Rev. Lett. **117**, 047003 (2016).

[29] K. Takubo, Y. Yokoyama, H. Wadati, S. Iwasaki, T. Mizokawa, T. Boyko, R. Sutarto, F. He, K. Hashizume, S. Imaizumi, T. Aoyama, Y. Imai, and K. Ohgushi, Phys. Rev. B **96**, 115157 (2017).

[30] P. Materne, W. Bi, J. Zhao, M. Y. Hu, M. L. Amigó, S. Seiro, S. Aswartham, B. Büchner, and E. E. Alp, Phys. Rev. B **99**, 020505(R) (2019).

[31] N. D. Patel, A. Nocera, G. Alvarez, A. Moreo, S. Johnston, and E. Dagotto, Commun. Phys. **2**, 64 (2019).

[32] L. Craco and S. Leoni, Phys. Rev. B **101**, 245133 (2020).

[33] T. Yamauchi, Y. Hirata, Y. Ueda, and K. Ohgushi, Phys. Rev. Lett. **115**, 246402 (2015).

[34] H. Takahashi, A. Sugimoto, Y. Nambu, T. Yamauchi, Y. Hirata, T. Kawakami, M. Avdeev, K. Matsubayashi, F. Du, C. Kawashima, H. Soeda, S. Nakano, Y. Uwatoko, Y. Ueda, T. J. Sato, and K. Ohgushi, Nat. Mat. **14**, 1008 (2015).

[35] J. Ying, H. Lei, C. Petrovic, Y. Xiao, and V. V. Struzhkin, Phys. Rev. B **95**, 241109(R) (2017).

[36] Y. Zhang, L-F. Lin, J-J. Zhang, E. Dagotto, and S. Dong, Phys. Rev. B **95**, 115154 (2017).

[37] Y. Zhang, L-F. Lin, J.-J. Zhang, E. Dagotto, and S. Dong, Phys. Rev. B **97**, 045119 (2018).

[38] T. Hawai, Y. Nambu, K. Ohgushi, F. Du, Y. Hirata, M. Avdeev, Y. Uwatoko, Y. Sekine, H. Fukazawa, J. Ma, S. Chi, Y. Ueda, H. Yoshizawa, and T. J. Sato, Phys. Rev. B **91**, 184416 (2015).

[39] M. Wang, M. Yi, S. Jin, H. Jiang, Y. Song, H. Luo, A. D. Christianson, C. de la Cruz, E. Bourret-Courchesne, D.-X. Yao, D. H. Lee, and R. J. Birgeneau, Phys. Rev. B **94**, 041111(R) (2016).

[40] M. Wang, S. J. Jin, Ming Yi, Yu Song, H. C. Jiang, W. L. Zhang, H. L. Sun, H. Q. Luo, A. D. Christianson, E. Bourret-Courchesne, D. H. Lee, Dao-Xin Yao, and R. J. Birgeneau, Phys. Rev. B **95**, 060502(R) (2017).

[41] M. Mourigal, S. Wu, M. B. Stone, J. R. Neilson, J. M. Caron, T. M. McQueen, and C. L. Broholm, Phys. Rev. Lett. **115**, 047401 (2015).

[42] J. M. Caron, J. R. Neilson, D. C. Miller, A. Llobet, and T. M. McQueen, Phys. Rev. B **84**, 180409(R) (2011).

[43] Y. Nambu, K. Ohgushi, S. Suzuki, F. Du, M. Avdeev, Y. Uwatoko, K. Munakata, H. Fukazawa, S. Chi, Y. Ueda, and T. J. Sato, Phys. Rev. B **85**, 064413 (2012).

[44] S. Wu, J. Yin, T. Smart, A. Acharya, C. L. Bull, N. P. Funnell, T. R. Forrest, G. Simutis, R. Khasanov, S. K. Lewin, M. Wang, B. A. Frandsen, R. Jeanloz, and R. J. Birgeneau, Phys. Rev. B **100**, 214511 (2019).

[45] M. Wang, C. Fang, D.-X. Yao, G. Tan, L. W. Harriger, Y. Song, T. Netherton, C. Zhang, M. Wang, M. B. Stone, W. Tian, J. Hu, and P. Dai, Nat. Comm. **2**, 580 (2011).

[46] B. Wei, H. Qing-Zhen, C. Gen-Fu, M. A. Green, W. Du-Ming, H. Jun-Bao, and Q. Yi-Ming, Chin. Phys. Lett. **28**, 086104 (2011).

[47] Y.-Z. You, H. Yao, and D.-H. Lee, Phys. Rev. B **84**, 020406(R) (2011).

[48] R. Yu, P. Goswami, and Q. Si, Phys. Rev. B **84**, 094451 (2011).

[49] J. Guo, S. Jin, G. Wang, S. Wang, K. Zhu, T. Zhou, M. He, and X. Chen Phys. Rev. B **82**, 180520(R) (2010).

[50] F. Ye, S. Chi, Wei Bao, X. F. Wang, J. J. Ying, X. H. Chen, H. D. Wang, C. H. Dong, and M. Fang, Phys. Rev. Lett. **107**, 137003 (2011).

[51] J. K. Glasbrenner, I. I. Mazin, Harald O. Jeschke, P. J. Hirschfeld, R. M. Fernandes, and R. Valentí , Nat. Phys. **11**, 953 (2015).

[52] H. Ruiz, Y. Wang, B. Moritz, A. Baum, R. Hackl, and T. P. Devereaux, Phys. Rev. B **99**, 125130 (2019).

[53] B. Pandey, L.-F. Lin, R. Soni, N. Kaushal, J. Herbrych, G. Alvarez, and E. Dagotto, Phys. Rev. B **102**, 035149 (2020).

[54] L.-F. Lin, Y. Zhang, G. Alvarez, A. Moreo, and E. Dagotto, Phys. Rev. Lett. **127**, 077204 (2021).

[55] Y. Zhang, L-F. Lin, A. Moreo, S. Dong, and E. Dagotto, Phys. Rev. B **100**, 184419 (2019).

[56] Y. Zhang, L-F. Lin, A. Moreo, S. Dong, and E. Dagotto, Phys. Rev. B **101**, 144417 (2020).

[57] Q. Luo, A. Nicholson, J. Riera, D.-X. Yao, A. Moreo, and E. Dagotto, Phys. Rev. B **84**, 140506(R) (2011)

[58] Q. Luo and E. Dagotto, Phys. Rev. B **89**, 045115 (2014).

[59] Q. Luo, A. Nicholson, J. Rincón, S. Liang, J. Riera, G. Alvarez, L. Wang, W. Ku, G. D. Samolyuk, A. Moreo, and E. Dagotto, Phys. Rev. B **87**, 024404 (2013).

[60] W.-G. Yin, C.-H. Lin, and W. Ku, Phys. Rev. B **86**, 081106(R) (2012).

[61] S. Dong, J.-M. Liu, and E. Dagotto, Phys. Rev. Lett. **113**, 187204 (2014).

[62] A. Isidori, M. Berović, L. Fanfarillo, L. de' Medici, M. Fabrizio, and M. Capone, Phys. Rev. Lett. **122**, 186401 (2019).

[63] S. R. White, Phys. Rev. Lett. **69**, 2863 (1992).

[64] U. Schollwöck, Rev. Mod. Phys. **77**, 259 (2005).

[65] G. Alvarez, Comput. Phys. Commun. **180**, 1572 (2009).

[66] S. R. White, Phys. Rev. B **72**, 180403(R) (2005).

[67] E. Jeckelmann, Phys. Rev. B **66**, 045114 (2002).

[68] H. Benthien and E. Jeckelmann, Phys. Rev. B **75**, 205128 (2007).

[69] A. Nocera and G. Alvarez, Phys. Rev. E **94**, 053308 (2016).

[70] T. D. Kühner and S. R. White, Phys. Rev. B **60**, 335 (1999).

[71] J. Rincón, A. Moreo, G. Alvarez, and E. Dagotto, Phys. Rev. Lett. **112**, 106405 (2014).

[72] J. R. Schrieffer and P. A. Wolff, Phys. Rev. **149**, 491 (1966).

[73] E. Dagotto, *Nanoscale Phase Separation and Colossal Magnetoresistance*, Springer Berlin, Heidelberg (2003).

[74] J. C. Xavier, R. G. Pereira, E. Miranda, and I. Affleck, Phys. Rev. Lett. **90**, 247204 (2003).

[75] G. W. Winkler, M. Ganahl, D. Schuricht, H. G. Evertz, and S. Andergassen, New. J. Phys. **19**, 063009 (2017).

[76] S. R. Elliott, and M. Franz, Rev. Mod. Phys. **87**, 137 (2015).

[77] R. Pawlak, S. Hoffman, J. Klinovaja, D. Loss, and E. Meyer, Prog. Part. Nucl. Phys. **107**, 1 (2014).

[78] B. Braunecker, G. I. Japaridze, J. Klinovaja, and D. Loss, Phys. Rev. B. **82**, 045127 (2010).

[79] D. Wang, L. Kong, P. Fan, H. Chen, S. Zhu, W. Liu, L. Cao, Y. Sun, S. Du, J. Schneeloch, R. Zhong, G. Gu, L. Fu, H. Ding, and H.-J. Gao, Science **362**, 333 (2018).

[80] P. Zhang, K. Yaji, T. Hashimoto, Y. Ota, T. Kondo, K. Okazaki, Z. Wang, J. Wen, G. D. Gu, H. Ding, and S. Shin, Science **360**, 182 (2018).

[81] T. Machida, Y. Sun, S. Pyon, S. Takeda, Y. Kohsaka, T. Hanaguri, T. Sasagawa, and T. Tamegai, Nat. Mater. **18**, 811 (2019).

[82] Z. Wang, J. O. Rodriguez, L. Jiao, S. Howard, M. Graham, G. D. Gu, T. Hughes, D. K. Morr, and V. Madhavan, Science **367**, 104 (2020).

[83] C. Chen, K. Jiang, Y. Zhang, C. Liu, Y. Liu, Z. Wang, and Jian Wang, Nat. Phys. **16**, 536 (2020).

Other scientific and research achievements

3.1 JCR publication list

Total number of publications indexed in Journal Citation Reports: 37

- Annalen der Physik (2020 IF: 3.276) $\times 1$
- Differential Equations and Dynamical Systems (2020 IF: 1.260) $\times 1$
- Nature Communications (2020 IF: 14.920) $\times 2$
- Physical Review A (2020 IF: 3.140) $\times 1$
- Physical Review B (2020 IF: 4.036) $\times 25$
- Physical Review E (2020 IF: 2.529) $\times 1$
- Physical Review Letters (2020 IF: 9.161) $\times 4$
- Physical Review Research (2020 IF: 0.740) $\times 1$
- Proceedings of the National Academy of Sciences of the USA (2020 IF: 11.200) $\times 1$

List of publications **not included** in the achievement described in Chapter 2:

A31 *Magnetization dynamics fingerprints of an excitonic condensate t_{2g}^4 magnet*
N. Kaushal, J. Herbrych, G. Alvarez, and E. Dagotto,
Phys. Rev. B **104**, 235135 (2021).

A30 *Coexistence of diffusive and ballistic transport in integrable quantum lattice models*
P. Prelovšek, M. Mierzejewski, and J. Herbrych,
Phys. Rev. B **104**, 115163 (2021).

A29 *Diffusion in the Anderson model in higher dimensions*,
P. Prelovšek and J. Herbrych,
Phys. Rev. B **103**, L241107 (2021).

A28 *Ballistic transport in integrable lattice models with degenerate spectra*,
M. Mierzejewski, J. Herbrych, and P. Prelovšek,
Phys. Rev. B **103**, 235115 (2021).

A27 *Resistivity and its fluctuations in disordered many-body systems: from chains to planes*,
M. Mierzejewski, M. Środa, J. Herbrych, and P. Prelovšek,
Phys. Rev. B **102**, 161111(R) (2020).

A26 *Prediction of exotic magnetic states in the alkali metal quasi-one-dimensional iron selenide compound Na_2FeSe_2*,
B. Pandey, L.-F. Lin, R. Soni, N. Kaushal, J. Herbrych, G. Alvarez, and E. Dagotto,
Phys. Rev. B **102**, 035149 (2020).

A25 *Vanishing Wilson ratio as the hallmark of quantum spin-liquid models*,
P. Prelovšek, K. Morita, T. Tohyama, and J. Herbrych,
Phys. Rev. Research **2**, 023024 (2020).

A24 *Inelastic neutron scattering study of the anisotropic $S = 1$ spin chain $[Ni(HF_2)(3\text{-}Clpyridine)_4]BF_4$*,
D. M. Pajerowski, J. L. Manson, J. Herbrych, J. Bendix, A. P. Podlesnyak, J. M. Cain, and M. W. Meisel,
Phys. Rev. B **101**, 094431 (2020).

A23 *Charge-density-wave melting in the one-dimensional Holstein model*,
J. Stolpp, J. Herbrych, F. Dorfner, E. Dagotto, and F. Heidrich-Meisner,
Phys. Rev. B **101**, 035134 (2020).

A22 *Magnetization and energy dynamics in spin ladders: Evidence of diffusion in time, frequency, position, and momentum*,
J. Richter, F. Jin, L. Knipschild, J. Herbrych, H. De Raedt, K. Michielsen, J. Gemmer, and R. Steinigeweg,
Phys. Rev. B **99**, 144422 (2019).

A21 *Sudden removal of a static force in a disordered system: Induced dynamics, thermalization, and transport*,
J. Richter, J. Herbrych, and R. Steinigeweg,
Phys. Rev. B **98**, 134302 (2018).

A20 *Non-equilibrium mass transport in the Fermi-Hubbard model*,
S. Scherg, T. Kohlert, J. Herbrych, J. Stolpp, P. Bordia, U. Schneider, F. Heidrich-Meisner, I. Bloch, and M. Aidelsburger,
Phys. Rev. Lett. **121**, 130402 (2018).

A19 *Density-matrix renormalization group study of a three-orbital Hubbard model with spin-orbit coupling in one dimension*,
N. Kaushal, J. Herbrych, A. Nocera, G. Alvarez, A. Moreo, F. A. Reboredo, and E. Dagotto,
Phys. Rev. B **96**, 155111 (2017).

A18 *Efficiency of fermionic quantum distillation*,
J. Herbrych, A. E. Feiguin, E. Dagotto, and F. Heidrich-Meisner,
Phys. Rev. A **96**, 033617 (2017).

A17 *Possible bicollinear nematic state with monoclinic lattice distortions in iron telluride compounds*,
C. B. Bishop, J. Herbrych, E. Dagotto, and A. Moreo,
Phys. Rev. B **96**, 035144 (2017).

A16 *Self-consistent approach to many-body localization and subdiffusion*,
P. Prelovšek and J. Herbrych,
Phys. Rev. B **96**, 035130 (2017).

A15 *Dynamics of locally coupled oscillators with next-nearest-neighbor interaction*,
J. Herbrych, A. G. Chazirakis, N. Christakis, and J. J. P. Veerman,
Differ. Equ. & Dyn. Syst., **29**, 487 (2021).

A14 *Density correlations and transport in models of many-body localization*,
P. Prelovšek, M. Mierzejewski, O. Barišić, and J. Herbrych,
Ann. Phys. (Berlin) **529**, 1600362 (2017).

A13 *Interaction-induced weakening of localization in few-particle disordered Heisenberg chains*,
D. Schmidtke, R. Steinigeweg, J. Herbrych, and J. Gemmer,
Phys. Rev. B **95**, 134201 (2017).

A12 *Effective realization of random magnetic fields in compounds with large single-ion anisotropy*,
J. Herbrych and J. Kokalj,
Phys. Rev. B **95**, 125129 (2017).

A11 *Universal dynamics of density correlations at the transition to many-body localized state*,
M. Mierzejewski, J. Herbrych, and P. Prelovšek,
Phys. Rev. B **94**, 224207 (2016).

A10 *Typicality approach to the optical conductivity in thermal and many-body localized phases*,
R. Steinigeweg, J. Herbrych, F. Pollmann, and W. Brenig,
Phys. Rev. B **94**, 180401(R) (2016).

A9 *Light induced magnetization in a spin $S = 1$ easy-plane antiferromagnetic chain*,
J. Herbrych and X. Zotos,
Phys. Rev. B **93**, 134412 (2016).

A8 *Heat conductivity of the Heisenberg spin-$1/2$ ladder: From weak to strong breaking of integrability*,
R. Steinigeweg, J. Herbrych, X. Zotos, and W. Brenig,
Phys. Rev. Lett. **116**, 017202 (2016).

A7 *Antiferromagnetic order in weakly coupled random spin chains*,
J. Kokalj, J. Herbrych, A. Zheludev, and P. Prelovšek,
Phys. Rev. B **91**, 155147 (2015).

A6 *Effective $S = 1/2$ description of the $S = 1$ chain with strong easy plane anisotropy*,
C. Psaroudaki, J. Herbrych, J. Karadamoglou, P. Prelovšek, X. Zotos, and N. Papanicolaou,
Phys. Rev. B **89**, 224418 (2014).

Publications before obtaining the PhD title:

A5 *Local spin relaxation within the random Heisenberg chain*,
J. Herbrych, J. Kokalj, and P. Prelovšek,
Phys. Rev. Lett. **111**, 147203 (2013).

A4 *Eigenstate thermalization in isolated spin-chain systems*,
R. Steinigeweg, J. Herbrych, and P. Prelovšek,
Phys. Rev. E **87**, 012118 (2013).

A3 *Spin hydrodynamics in the $S = 1/2$ anisotropic Heisenberg chain*,
J. Herbrych, R. Steinigeweg, and P. Prelovšek,
Phys. Rev. B **86**, 115106 (2012).

A2 *Coexistence of anomalous and normal diffusion in integrable Mott insulators*,
R. Steinigeweg, J. Herbrych, P. Prelovšek, and M. Mierzejewski,
Phys. Rev. B **85**, 214409 (2012).

A1 *Finite-temperature Drude weight within the anisotropic Heisenberg chain*,
J. Herbrych, P. Prelovšek, and X. Zotos,
Phys. Rev. B **84**, 155125 (2011).

Brief description

Transport in low-dimensional quantum systems:
Ref. [A1-A9,A18,A20,A22-A24,A28,A30].
Transport in many-body systems of interacting fermions established several novel - entirely quantum - aspects going well beyond usual weak-scattering or Boltzmann-type approaches. Such behavior is especially pronounced in the system with reduced dimensionality (e.g., in 1D chains and quasi-1D ladders). Prominent fundamental models and an experimentally relevant example of such a phenomenon are the one-dimensional single-orbital Hubbard and antiferromagnetic Heisenberg models. In a series of publications, I investigated quantities related to the transport properties (e.g., via the linear response theory) of various low-dimensional strongly-correlated systems, e.g., the dynamical optical conductivity $\sigma(\omega)$, the dynamical structure factor $S(q,\omega)$, or the diffusion constant. Furthermore, I also investigated related questions in the non-equilibrium setups, i.e., as the response of the system after the quench.

Many-body localization:
Ref. [A10-A14,A16,A21,A27,A29].
The phenomenon of many-body localization (MBL) deals with a challenging interplay of the disorder and interaction in many-body quantum systems, opening also the fundamental questions on the statistical description of such systems. It is suggested by numerous numerical studies that prototype 1D models on increasing disorder reveal the transition/crossover from an ergodic behavior to a localized regime characterized by several criteria: change in level statistics and spectral properties, slow growth of entanglement entropy, vanishing dc conductivities, and transport, nonergodic behavior of local correlations and the absence of thermalization, the latter being also the experimental probe in cold-atom systems. My work on this topic focuses on the properties of the dynamical correlations within a "standard model of MBL", i.e., 1D Heisenberg model of interacting spins or, equivalently via Jordan-Wigner transformation 1D model of interacting spinless fermions.

Study of multiorbital models:
Ref. [A17,A19,A26,A31].
My interest in the physics of multiorbital goes beyond the one described in Chapter 2 as a "scientific achievement". E.g., I studied the nematic order due to the monoclinic lattice distortions found in two-dimensional iron telluride. Also, I got interested in the effect of the spin-orbit coupling within the three-orbital Hubbard model, relevant for ruthenates or iridates. Finally, via the combination of density functional theory and density-matrix renormalization group calculations, I look for novel low-dimensional materials for which block orbital-selective Mott phase is relevant.

3.2 Bibliometric information

- Published articles according to Web of Science: 37

- Citation number according to Web of Science: 576 (490 without self-citations)
- Hirsch index according to Web of Science: 13
- Average citation per publication on the base of Web of Science: 15.57
- Total impact factor on the base of Web of Science: 241.596

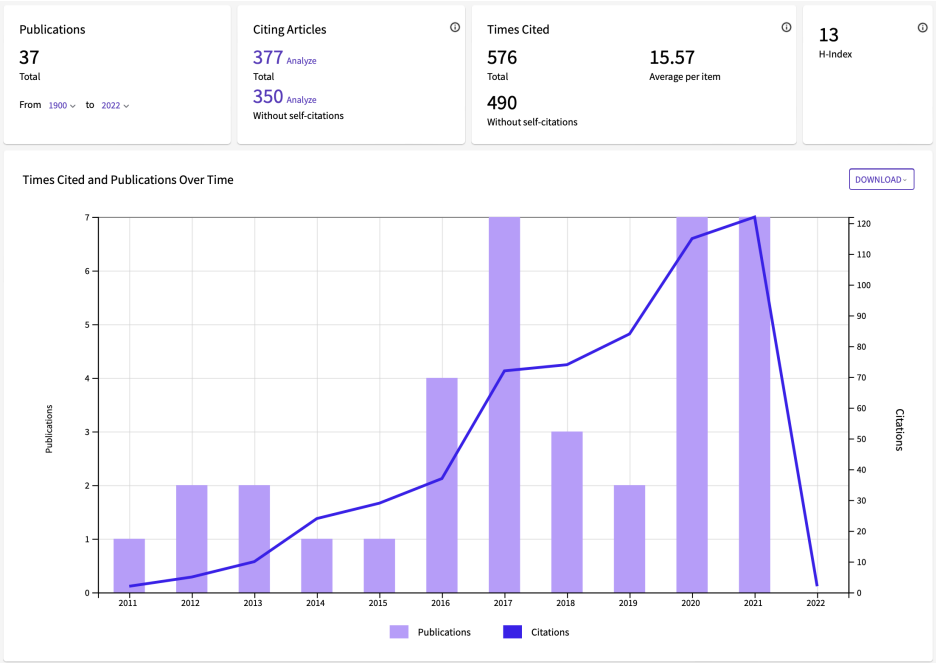

3.3 Research projects

- Principal Investigator in OPUS 18 project entitled *Magnetic properties of strongly-correlated multiorbital systems* founded by the National Science Centre (OPUS 18 2019/35/B/ST3/01207).
  The project is carried out at the Faculty of Fundamental Problems of Technology of Wrocław University of Science and Technology (2020-2022).
  Awarded founds: 198 600 zł.

- Principal Investigator in *Polish Returns* project founded by the Polish National Agency for Academic Exchange (PPN/PPO/2018/1/00035).
  The project is carried out at the Faculty of Fundamental Problems of Technology of Wrocław University of Science and Technology (2019-2022).
  Awarded founds: 1 125 000 zł.

3.4 Participation in European programs

- Participation in *Crete Center for Quantum Complexity and Nanotechnology* project founded by the EU Seventh Framework Programme (EU FP7 PEOPLE-ITN-2008 238475).
  The project was carried out in 2013-2016 at the University of Crete (Heraklion, Greece).
  Project Leader: Prof. Dr. Xenophon Zotos.

- Participation in *Low-dimensional quantum magnets for thermal management* project founded by the EU Marie Sklodowska-Curie Action (EU FP7 PEOPLE-ITN-2008 238475).
  The project was carried out in 2010-2013 at the Jožef Stefan Institute, Slovenia (Ljubljana).
  Project Leader: Prof. Dr. Peter Prelovšek.

3.5 Scientific talks

Oral presentations

- Nonequilibrium Quantum Workshop (Krvavec, Slovenia)
  December 2021
- APS March Meeting 2021 (virtual meeting)
  March 2021
- Nonequilibrium Quantum Workshop (Krvavec, Slovenia)
  December 2019
- Electron Correlation in Superconductors and Nanostructures (Odesa, Ukraine)
  October 2019
- International Workshop Korrelationstage (Dresden, Germany)
  September 2019
- APS March Meeting 2019 (Boston, USA)
  Marzec 2019
- 42nd International Conference of Theoretical Physics (Ustroń, Poland)
  September 2018
- APS March Meeting 2018 (Los Angeles, USA)
  March 2018
- Nonequilibrium Quantum Workshop (Krvavec, Slovenia)
  December 2017
- International Workshop Korrelationstage (Dresden, Germany)
  September 2017
- 40th International Conference of Theoretical Physics (Ustroń, Poland)
  September 2016
- Quantum Magnets 2015 (Kolymbari, Greece)
  September 2015
- Quantum Magnets 2013 (Kolymbari, Greece)
  September 2013
- 36th International Conference of Theoretical Physics (Ustroń, Poland)
  September 2012

Poster presentation

- Quantum Spin Dynamics (Dresden, Germany)
  September 2014
- Quantum Magnets 2013 (Kolymbari, Greece)
  September 2013
- 36th International Conference of Theoretical Physics (Ustroń, Poland)
  September 2012
- Dynamics and transport in quantum magnets, LOTHERM Summer School (Ljubljana, Slovenia)
  June 2011
- School on "Strongly correlated electronic systems, beyond Fermi liquid theory" (Les Houches, France)
  April 2011

Invited talks at the scientific institutions

- Polish Academy of Science - Institute of Physics (Warsaw, Poland)
  March 2021, November 2021
- Jožef Stefan Institute (Ljubljana, Slovenia)
  March 2014, March 2015, June 2016, September 2021
- Maria Curie-Skłodowska University Lublin (Lublin, Poland)
  May 2021
- University of Warsaw (Warsaw, Poland)
  November 2020
- Osnabrück University (Osnabrück, Germany)
  September 2014, June 2015, June 2016, November 2020
- University of Göttingen (Göttingen, Germany)
  July 2019
- Stuttgart University (Stuttgart, Germany)
  June 2019
- Ludwig Maximilian University of Munich (Munich, Germany)
  December 2017
- Wrocław University of Science and Technology (Wrocław, Poland)
  December 2017
- Joint Institute for Advanced Materials (Knoxville, USA)
  November 2017
- Technical University of Braunschweig (Braunschweig, Germany)
  May 2014

3.6 Membership in scientific societies

- American Physical Society

3.7 Refereeing in international journals

- Physical Review B (American Physical Society) - 4 reviews
- Physical Review Letters (American Physical Society) - 2 reviews
- Physical Review Research (American Physical Society) - 1 review
- New Journal of Physics (IOP Publishing) - 1 review
- Annalen der Physik (Wiley-VCH) - 1 review

3.8 Scientific collaborations

List of the most important scientific collaborations:

- Jožef Stefan Institute (Ljubljana, Slovenia)
  Prof. Dr. Peter Prelovsek, Dr. Jure Kokajl, Dr. Jernej Mravlje
- University of Crete (Heraklion, Greece)
  Prof. Dr. Xenophon Zotos
- University of Tennessee (Knoxville, USA)
  Prof. Dr. Elbio Dagotto, Prof. Dr. Adriana Moreo
- Oak Ridge National Laboratory (Oak Ridge, USA)
  Dr. Gonzalo Alvarez, Dr. Nitin Kaushal, Dr. Daniel Pajerowski
- Osnabrück University (Osnabrück, Germany)
  Prof. Dr. Robin Steinigeweg
- University of Göttingen (Göttingen, Germany)
  Prof. Dr. Fabian Heidrich-Meisner, Dr. Salvatore R. Manmana
- California Institute of Technology (Pasadena, USA)
  Dr. Christina Psaroudaki
- University of British Columbia (Vancouver, Canada)
  Dr. Alberto Nocera
- University of Warsaw (Warszawa, Poland)
  Dr. hab. Krzysztof Wohlfeld
- Wrocław University of Science and Technology (Wrocław, Poland)
  Prof. Dr. hab. Marcin Mierzejewski

Didactic achievements and administrative activity

4.1 Didactic activity

2020/2021 Models of strongly correlated systems
Lecture for 3rd year of MSc studies (Polish language)
Wrocław University of Science and Technology (Wrocław, Poland)

2020/2021 Numerical methods for quantum systems
Laboratory for 1st year of MSc studies (Polish language)
Wrocław University of Science and Technology (Wrocław, Poland)

2020/2021 Statistical Physics
Laboratory for 1st year of MSc studies (English language)
Wrocław University of Science and Technology (Wrocław, Poland)

2019/2020 Models of strongly correlated systems
Lecture for 3rd year of MSc studies (Polish language)
Wrocław University of Science and Technology (Wrocław, Poland)

2019/2020 Numerical methods for quantum systems
Laboratory for 1st year of MSc studies (Polish language)
Wrocław University of Science and Technology (Wrocław, Poland)

4.2 Scientific supervision of students and PhD students

- Leader of the research group carrying out research within the *Polish Returns* project founded by the Polish National Agency for Academic Exchange (one contractor) and the *Magnetic properties of strongly correlated multi-orbital systems* project founded by the National Science Center (two contractors).
- Secondary supervisor in one doctoral thesis. The topic of the dissertation: "Electronic and magnetic properties of low-dimensional strongly correlated multiorbital systems".
- Supervisor of 2 master's theses.
- Supervisor of 2 diploma theses.
- Tutor of the individual course of study of 2 students.

4.3 Administrative activity

- Member of the faculty council of the Faculty of Fundamental Problems of Technology of Wrocław University of Science and Technology.

- Member of the didactic committee for "Quantum Engineering" studies at the Faculty of Fundamental Problems of Technology of Wrocław University of Science and Technology.
- Supervisor of the scientific club "Nabla" at the Faculty of Fundamental Problems of Technology of Wrocław University of Science and Technology (2020-2021).
- Participation in committees for master's and diploma theses defense.